RPC INDUSTRIES

RPC-80-11403-80-FR

PHASE TRANSITION COOLED WINDOW STUDIES FOR HIGH AVERAGE POWER ELECTRON GUNS

FINAL REPORT

Sponsored by

Defense Advanced Research Projects Agency (DOD)
ARPA Order No. 3498, Amendment No. 6

This research was supported by the Defense Research Projects Agency of the Department of Defense and was monitored by the U.S. Army Missile Command under Contract Number DAAK40-79-C-0258.

December, 1980

P.O. BOX 3308, HAYWARD, CALIFORNIA 94540, TELEPHONE (415) 785-8040, TELEX 335-473

UNCLASSIFIED

SECURITY CLASSIFICATION OF THIS PAGE (When Data Entered)

REPORT DOCUMENTATION PAGE	READ INSTRUCTIONS BEFORE COMPLETING FORM
1. REPORT NUMBER	2. GOVT ACCESSION NO. AD-A100 630 / 3. RECIPIENT'S CATALOG NUMBER
4. TITLE (and Subtitle) (6) Phase Transition Cooled Window Studies for High Average Power Electron Guns. (9) Final Report.	5. TYPE OF REPORT & PERIOD COVERED Technical Report / 6. PERFORMING ORG. REPORT NUMBER
7. AUTHOR(s) (10) G. Loda, D. Forcier	8. CONTRACT OR GRANT NUMBER(s) (15) DAAK40-79-C-0258 / ARPA Order-3498
9. PERFORMING ORGANIZATION NAME AND ADDRESS RPC Industries (New) P.O. Box 3306 Hayward, CA 94540	10. PROGRAM ELEMENT, PROJECT, TASK AREA & WORK UNIT NUMBERS (12) 88
11. CONTROLLING OFFICE NAME AND ADDRESS (11) Headquarters U.S. Army Missile Command Attn: DRSMI-IYD Redstone Arsenal, AL 35809	12. REPORT DATE December, 1980 / 13. NUMBER OF PAGES 80
14. MONITORING AGENCY NAME & ADDRESS (if different from Controlling Office) (14) RPC-80-11403-84-FR	15. SECURITY CLASS. (of this report) UNCLASSIFIED / 15a. DECLASSIFICATION/DOWNGRADING SCHEDULE
16. DISTRIBUTION STATEMENT (of this Report) DISTRIBUTION STATEMENT A Approved for public release;	
17. DISTRIBUTION STATEMENT (of the abstract entered in Block 20, if different from Report) DTIC ELECTE JUN 26 1981	
18. SUPPLEMENTARY NOTES	
19. KEY WORDS (Continue on reverse side if necessary and identify by block number) High energy lasers; Electron guns; Electron beam pumped lasers; Electron beam windows; Aerosol cooling	
20. ABSTRACT (Continue on reverse side if necessary and identify by block number) The window used to transmit electron beams for use in high average power UV/visible lasers has been a critical technology issue. The window structure must satisfy a number of conflicting requirements including: vacuum integrity, strength to overcome both the static and dynamic pressure loads of the laser gas and a low mass density to minimize energy loss by the electron beam. In addition, it must not perturb the laser gas flow and must be able to dissipate the power deposited by the electron beam. (over) 412404	

DD FORM 1 JAN 73 1473 EDITION OF 1 NOV 65 IS OBSOLETE

UNCLASSIFIED

SECURITY CLASSIFICATION OF THIS PAGE (When Data Entered)

Block 20 (continued)

Prior to this program the technology base for cooling windows was thermal conduction cooling through the foil to a cooled perimeter support or by forced convection cooling in either a dual foil or single foil geometry. Practical limits for both these techniques limited the deposited energy of the electron beam to approximately 10 watts per square centimeter. Neither technique could be made to scale to power densities significantly greater than this number. A variation on the convective cooled type of structure is the introduction of mixed phase flow. By injecting a two phase flow (for example, liquid droplets in a gas stream, an aerosol) between the dual foil structure, heat transfer will occur by a phase transition from liquid to gas. The heat of vaporization for most liquids is very large (λ water = 2.5 kJ/gm) and consequently a large amount of heat can be dissipated for a small amount of liquid.

Two experiments were undertaken to demonstrate the applicability of phase transition cooling for high power laser systems. In the first of these a full width 50 cm module was tested with a constant input heat source. The second experiment used a pulsed e-beam source to demonstrate cooling for a low duty cycle high peak power pulsed system.

The first set of experiments demonstrated the following:

1. The mean temperature of the foil could be altered by changing liquid. For water, the temperature is 100°C; for ethylene glycol the temperature is 200°C, corresponding to their vaporization temperatures at atmospheric pressure.

2. Power transfer capabilities in excess of 100 W/cm^2/foil surface were demonstrated with liquid utilization efficiency of 25%.

The second set of experiments were designed to confirm these previous measurements where the heating was pulsed rather than continuous. These pulsed heating experiments demonstrated a two rate cooling time history. The first rate is for ablation of a water film that builds up between pulses and the second rate results from interaction between the aerosol flow and the foils. The overall performance was as predicted from the constant heat flux measurements.

1. Mean temperature was on the order of 100°C for water.

2. Efficiency, although not optimized for nozzle/channel geometry was again on the order of 25%.

3. Power transfer capabilities were in excess of 100 W/cm^2/foil surface.

In summary, the applicability of phase transition cooling for a dual foil geometry was clearly demonstrated. Cooling rates in excess of 100 W/cm^2/foil surface with mass flow rates consistent with low areal mass density were achieved. This represents a factor of ten improvement over prexisting state of the art.

RPC INDUSTRIES

RPC-80-11403-80-FR

PHASE TRANSITION COOLED WINDOW
STUDIES FOR HIGH AVERAGE
POWER ELECTRON GUNS

FINAL REPORT

Sponsored by

Defense Advanced Research Projects Agency (DOD)
ARPA Order No. 3498, Amendment No. 6

This research was supported by the Defense Research Projects Agency of the Department of Defense and was monitored by the U.S. Army Missile Command under Contract Number DAAK40-79-C-0258.

December, 1980

P.O. BOX 3306, HAYWARD, CALIFORNIA 94540, TELEPHONE (415) 785-8040, TELEX 335-473

TABLE OF CONTENTS

Section 1	Introduction	1
Section 2	Technical Discussion	5
2.0	Background	5
	2.1 Thermal Interaction	12
	2.2 Pulsed Loads	15
	2.3 Efficiency	17
Section 3	Experimental Apparatus and Techniques	18
	3.1 The Simulation Test Cell	18
	3.2 Laser Test Cell	35
Section 4	Experimental Results	52
	4.1 Simulated Foil Tests 100°C	52
	4.2 Electron Beam Tests	67
	4.3 Electron Beam Tests	67

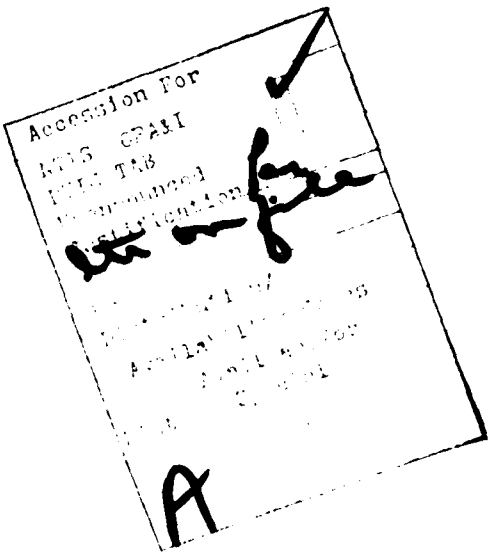

LIST OF FIGURES

Fig. 2.1	Phase Transition Cooling Demonstration Experiment	8
Fig. 2.2	Power Transfer for Phase Transition Cooling	9
Fig. 2.3	Dual Foil Structure	10
Fig. 2.4	Alternative Dual Foil Structure	11
Fig. 2.5	Cooling of Pulse Heated Foils	16
Fig. 3.1	Copper Block Modular Unit	20
Fig. 3.2	Representation of Full Length Simulation Test Cell	21
Fig. 3.3	Simulation Test Cells in Stacked Configuration	23
Fig. 3.4	SCR Current Control Unit	24
Fig. 3.5	Heat Flow in Stainless Steel Overlay	25
Fig. 3.6	Two Nozzle Assembly	28
Fig. 3.7	Schematic of Air and Water/Liquid Supply System	29
Fig. 3.8	Schematic of Laser Light Scattering Diagnostic	32
Fig. 3.9	Heat Transfer Characteristics	33
Fig. 3.10	Infrared Bandwidth Detected by Scanner and Absorption by Water in the Critical Bandwidth	34
Fig. 3.11	Laser Test Cell Assembly	36
Fig. 3.12	Window Plate for Laser Test Cell	38
Fig. 3.13	Laser Test Cell	39
Fig. 3.14	Block Diagram of Gun Circuit	40
Fig. 3.15	Test Unit Schematic	42
Fig. 3.16	Gun Test Chamber	43
Fig. 3.17	Complete Test Unit	44
Fig. 3.18	Cathode Holder	45
Fig. 3.19	Spark Cathode, 16 Sites/cm^2	46
Fig. 3.20	Laser Test Cell Nozzle Assembly	47
Fig. 3.21	Window Foil with Thermocouples Attached	49
Fig. 3.22	Response Times of Five Mil and Three Mil Thermocouples	50

Fig. 4.1	Power Transfer Characteristics	53
Fig. 4.2	Water Utilization Efficiency (Two blocks, single sided heating)	54
Fig. 4.3	Independence of Temperature on Power Loading	56
Fig. 4.4	Temperature Distribution	59
Fig. 4.5	Water Utilization Efficiency (Four blocks, single sided heating)	60
Fig. 4.6	Gas Cooling	61
Fig. 4.7	Water Utilization Efficiency (Two blocks, double sided heating)	62
Fig. 4.8	Maximum Power Transfer of Water	63
Fig. 4.9	Temperature Distribution - Turbulence Plate	65
Fig. 4.10	Temperature Distribution - Ethylene Glycol Coolant	68
Fig. 4.11	Ethylene Glycol Utilization Efficiency	69
Fig. 4.12	Light Scattering from Aerosol vs. Distance from Nozzles	66
Fig. 4.13	Thermocouple Time History	71
Fig. 4.14	Thermocouple Time History - Phase Transition Cooled	72
Fig. 4.15	Gas Cooling (Air Only) of Laser Test Cell - One Mil Stainless Steel Foil	73
Fig. 4.16	Failed Foil; Two Flat Spray Nozzles	76
Fig. 4.17	Failed Foil; No Aerosol Cooling	77
Fig. 4.18	Failed Foil; Two Round Spray Nozzles Convergent at a 7° Angle to the Center Line	79
Fig. 4.19	Aerosol Cooling with Single Round Spray Nozzle Mounted on the Center Line	80

LIST OF TABLES

Table 2.1	Vaporization Pressure of Water at Selected Temperatures	14
Table 4.1	Temperature Differential across Various Materials	57
Table 4.2	Test Data. Nozzle Configuration: 2 Full Cone Nozzles	75
Table 4.3	Test Data. Nozzle Configuration: 2 Flat Spray - Angled 7° Toward the Center Line	78
Table 4.4	Test Data. Nozzle Configuration: 1 Full Cone Spray on Center	81

SECTION I

INTRODUCTION AND SUMMARY

The window used to transmit electron beams for use in high average power UV/visible lasers has been a critical technology issue. The window structure must satisfy a number of conflicting requirements including: vacuum integrity, strength to overcome both the static and dynamic pressure loads of the laser gas and a low mass density to minimize energy loss by the electron beam. In addition, it must not perturb the laser gas flow and must be able to dissipate the power deposited by the electron beam. Having the ability to dissipate this power while satisfying the previously stated requirements will be the principle issue addressed in this report.

Prior to this program, the technology base for cooling windows, where the electron energies were relatively low, ($\leq$ 500 keV) was thermal conduction cooling through the foil to a cooled perimeter support or by forced convection cooling in either a dual foil or single foil geometry. Practical limits for both these techniques limited the deposited energy of the electron beam to approximately 10 watts per square centimeter. Neither technique could be made to scale to power densities significantly greater than this number. For example, in the conduction cooled system, in order to dissipate higher power densities, either the foil must be made thicker or the perimeter supports must be moved closer together. Both of these requirements would tend to decrease the total throughput energy of the beam and increase dissipation. In order to increase the cooling created by the forced convection, the flow velocity and turbulence must be increased As this velocity is increased, the pressure drop across the channel becomes too large for the mechanical structure to support.

A variation on the convective cooled type of structure is the introduction of mixed phase flow. By injecting a two phase flow (for example, liquid droplets in a gas stream, an aerosol) between the dual foil structure, heat transfer will occur by a phase transition from liquid to gas. The heat of vaporization for most liquids is very large (λ water = 2.5 kJ/gm) and consequently a large amount of heat can be dissipated for a small amount of liquid.

A small scale IR & D experiment was performed that demonstrated the basic behavior of phase transition cooling. Cooling rates in excess of 300 W/cm^2 were demonstrated by these tests for areas less than 1 cm^2. Several critical areas that were not investigated during that experiment included:

1. A determination of the areal mass density of the aerosol stream required to achieve a specific cooling rate in a laser window geometry.

2. A demonstration of the ability to adjust the mean temperature of the e-beam foil to match the laser cavity temperature.

The efficiency with which the liquid in the aerosol stream is converted to vapor is critical in determining the first item. This efficiency will depend on the geometry of the foil structure and the nozzle spray pattern and the consequent interaction of the phase transitioning flow with that structure. The areal density of the liquid is given by the expression:

$$\frac{1}{\eta\lambda}\left[\frac{\phi\ell}{v}\right]$$

where, ϕ power density

η efficiency of liquid utilization

λ heat of vaporization

ℓ length of flow dimension

v flow velocity

For example, if we require a cooling rate of 75 W/cm^2 (150 W/cm^2 total for both foils) over a 50 cm long flow dimension, the areal density of water required for a flow velocity of 10^4 cm/sec is

$$\frac{0.3 \text{ mg}}{\text{cm}^2} \quad \frac{1}{\eta}$$

If η is only 0.1, then the areal mass density is 3 mg/cm^2 as compared to an areal mass density of 11 mg/cm^2 for a nominal 1.0 mil titanium window.

In order not to produce density fluctuations within the laser cavity it is desired that the mean temperature of the foil closely corresponds to the mean temperature of the laser cavity. For some laser systems, the cavity temperature can approach 200°C, well beyond the practical limit for a water based system. A means of attaining these higher temperatures is to utilize liquids with higher vaporization temperatures.

Two experiments were undertaken to demonstrate the applicability of phase transition cooling for high power laser systems. In the first of these a full width 50 cm module was tested with a constant input heat source. The second experiment used a pulsed e-beam source to demonstrate cooling for a low duty cycle high peak power pulsed system.

The first set of experiments demonstrated the following:

1. The mean temperature of the foil could be altered by changing liquid. For water, the temperature is 100°C; for Ethylene Glycol the temperature is 200°C, corresponding to their vaporization temperatures at atmospheric pressure.

2. Efficiency of liquid utilization, η was of the order of 25%.

3. Power transfer capabilities in excess of 100 W/cm^2/foil surface were demonstrated at the above mentioned efficiency.

The second set of experiments (pulsed heating) were designed to confirm these previous measurements where the heating was pulsed rather than continuous. These pulsed heating experiments demonstrated a two rate cooling time history. The first rate is for ablation of a water film that builds up between pulses and the second rate results from interaction between the aerosol flow and the foils. The overall performance was as predicted from the constant heat flux measurements.

1. Mean temperature was on the order of 100°C for water.
2. Efficiency, although not optimized for nozzle/channel geometry was again on the order of 25%.
3. Power transfer capabilities were in excess of 100 W/cm^2/foil surface.

In summary, the applicability of phase transition cooling for a dual foil geometry was clearly demonstrated. Cooling rates in excess of 100 W/cm^2/foil surface with mass flow rates consistent with low areal mass density were achieved. This represents a factor of ten improvement over prexisting state of the art.

As a guide to specific future design or research on phase transition cooling the following is offered.

1. Only one nozzle per flow duct should be used to prevent interaction between the two nozzle flows.
2. Flow mixers positioned midway in the flow duct could be installed to increase utilization efficiencies for large aspect ratio systems.
3. Wetting agents added to the liquid, or surface treatment of the foil may be used to increase the instantaneous cooling by ablation of the water film.
4. The flush factor on aerosol flow be ≥ 1.
5. A combination of pressure and liquid mixture be used for achieving specific mean temperatures.

SECTION 2

TECHNICAL DISCUSSION

2.0 Background

The window required to transmit electron beam from the vacuum chamber into the high pressure excimer laser cell presents some very stringent requirements that must be simultaneously satisfied to ensure proper performance. These requirements include: (1) a low areal density for a high efficiency of transmission, (2) high strength to sustain high static and dynamic mechanical loads, (3) vacuum tight so as not to effect electron gun performance, (4) the above characteristics must be maintained after exposure to the radiation flux of the e-beam and repeated dynamic mechanical loads.

This last requirement eliminates the use of any polymer type materials, which have often been used in single shot experiments, from consideration for use on high average power devices. The choice of materials is necessarily limited to metal foils.

Because the foil presents a finite mass density to the electron beam, heating of the foil will take place as a result of the beam passage. For a rep rated application, this means that the heat must be removed from the foil during the interpulse time. Adiabatic cooling of the foil is of no use for run times anticipated. In providing a mechanism for removing heat from the foil structure it is necessary that the areal density is not increased and that a large geometrical blockage of the beam is not created. The effect of geometrical blockage can be somewhat alleviated by focusing the electron beam away from the blockage. However, in some cases very significant non-uniformities will be generated in the laser medium degrading its performance.

Prior to this program two different heat transfer mechanisms were in general use for cooling e-beam foils, conductive transfer and convective transfer. Demonstrated performance for both of the two techniques fell far short (2X to 10X) of the DARPA program requirements. For conduction

transfer, the heat generated in the foil was conducted to a perimeter support system which in turn was also cooled, usually with water. Because of the limited thermal conductivity of the foils with suitable strength to weight ratios at elevated temperatures, conductive cooling has been limited to a few tens of watts per square centimeter. To achieve transfer rates significantly greater than this requires very closely spaced perimeter supports which severely limits the overall electron transmission efficiency. The limit is easy to see for this type of cooling. If foil thickness is increased to facilitate heat conduction, the increased areal density will increase the heat load that must be dissipated.

Convective cooling has been accomplished either with a dual foil structure with water or gas flowing between the foils, or with a single foil whereby the flow of laser gas actively participates in the cooling of the foil. Relatively large heat transfer rates can be achieved with convective cooling with the fast flow of liquids. This technique has been used successfully for many years for high energy linear accelerators. In order to be useful for electrons with kinetic energies of interest here (200-600 keV), the thickness of the coolant flow must be on the order of 0.1 millimeters. For the large window structures in consideration here neither could the tolerances required be maintained, nor could the structure handle the large pressure drop required to achieve the necessary water flow rates.

Clearly, a new concept was required in order to solve the problem. The convective cooling mechanisms described above have many of the positive attributes required for cooling and overall system design. However, since each operates as a single phase system, they are quite limited to the heat that can be extracted by virtue of their specific heats. A mixed phase system, on the other hand, utilizing a phase change from liquid to gas, appeared to be a tractable solution. Changing phase from solid to gas, or solid to liquid or gas, does not appear to have particular advantage here; however, in some short run time systems the solid phase change may also be of interest. The amount of energy that can be extracted by a phase change is of course very large. For example, the amount of energy required to vaporize a cubic centimeter of water at room temperature is greater than 2.5 kJ.

If we were to consider a simple boiling water geometry we would be limited to the same water thickness listed above (0.1 Millimeters) and also we would encounter local burnout in the boiling system as the power densities reached 100 watts per square centimeter. This latter problem is a result of such vigorous boiling that the gas bubbles grow so large that the area in which the water actually contacts the surface is significantly reduced. A solution to this is to use an aerosol flow, that is, water droplets transported in an airstream.

To demonstrate the concept an experiment was performed under Systems, Science and Software IR & D to investigate an aerosol cooled substrate. The experimental setup is shown in Fig. 2.1 and consists of a copper block concentrator heated with a resistance heater with cooling performed by an aerosol stream over a small area in the block. The amount of heat lost in the system due to radiation or convection cooling was insignificant, therefore all the heat going into the block had to be carried away by the aerosol if the block was at a stable temperature. The results of these experiments are shown in Fig. 2.2. The physics of the situation are quite apparent. If the aerosol flow is sufficient, the substrate will reach and stabilize at a temperature equal to the boiling point of the liquid. If there is an excess of liquid, then the substrate temperature will be less than or equal to the vaporization temperature. If there is insufficient mass flow of the liquid, that is, all the liquid is vaporized, then the temperature of the substrate will become unbounded. If the mass flow of the liquid exactly balances the heat flux requirements, then the temperature of the block will be a singularity that will be equal to the vaporization temperature if approached from below, or undefined if approached from above.

Several concepts for adapting this cooling technique to the e-beam window are shown in Figs. 2.3 and 2.4. The aerosol flow occurs along the narrow dimension of the laser window which corresponds to 50 cm. The devices called e-beam shield/radiators are intended to limit the energy deposition into the supporting ribs and will be cooled by radiative transfer. In operation these radiators would become incandescent, however, they are

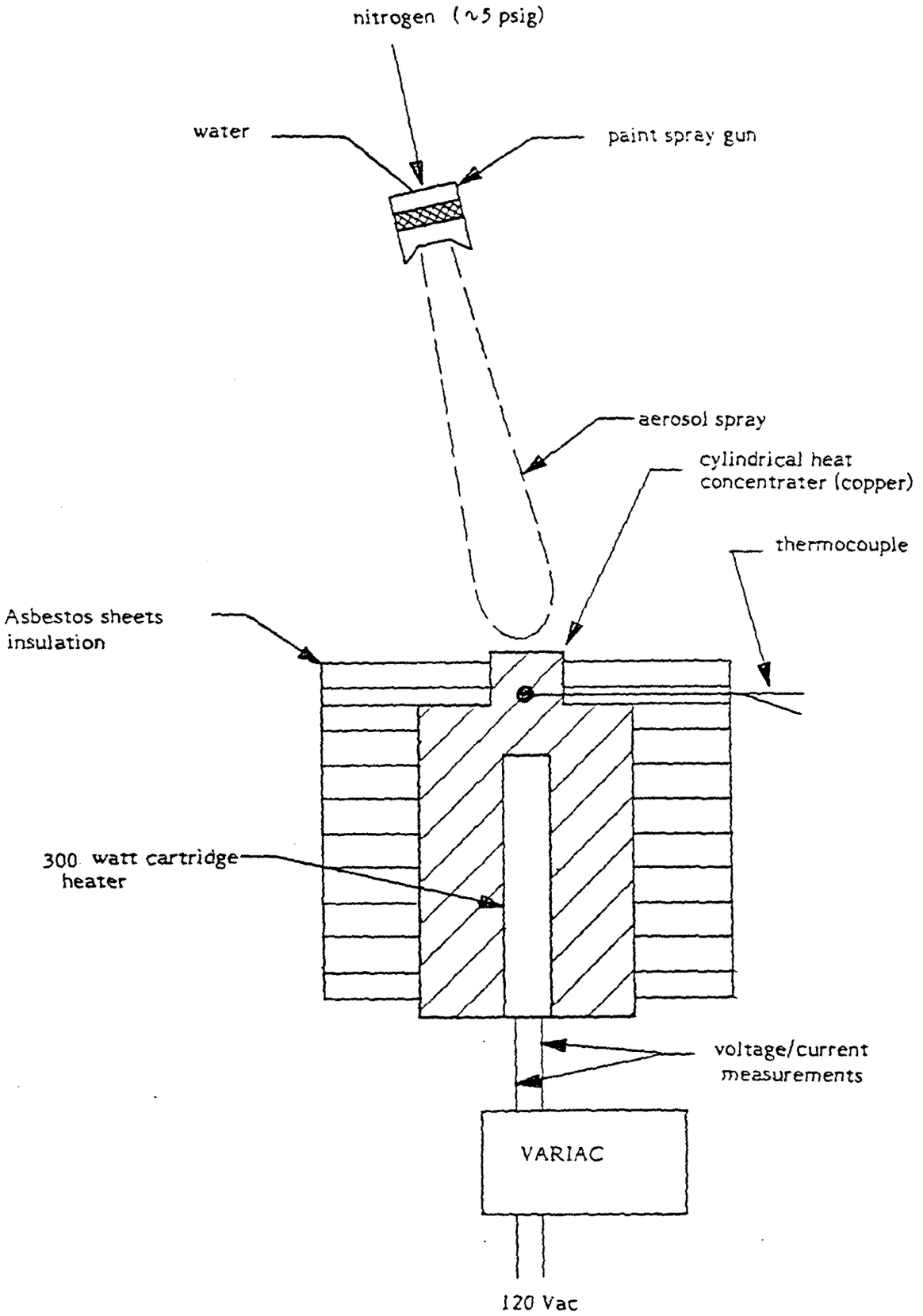

Fig. 2.1 Phase Transition Cooling Demonstration Experiment

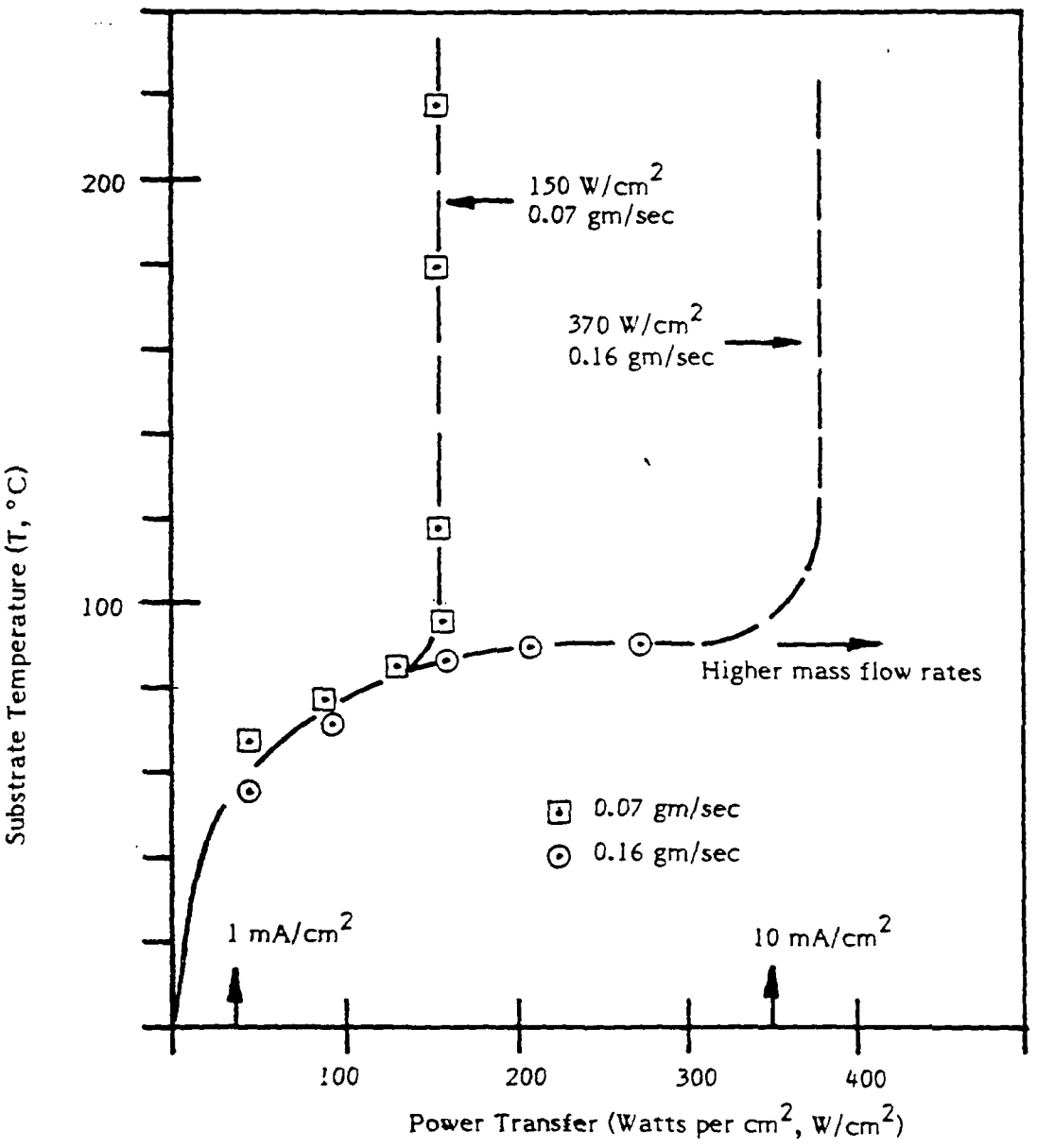

FIG. 2.2 POWER TRANSFER FOR PHASE TRANSITION COOLING

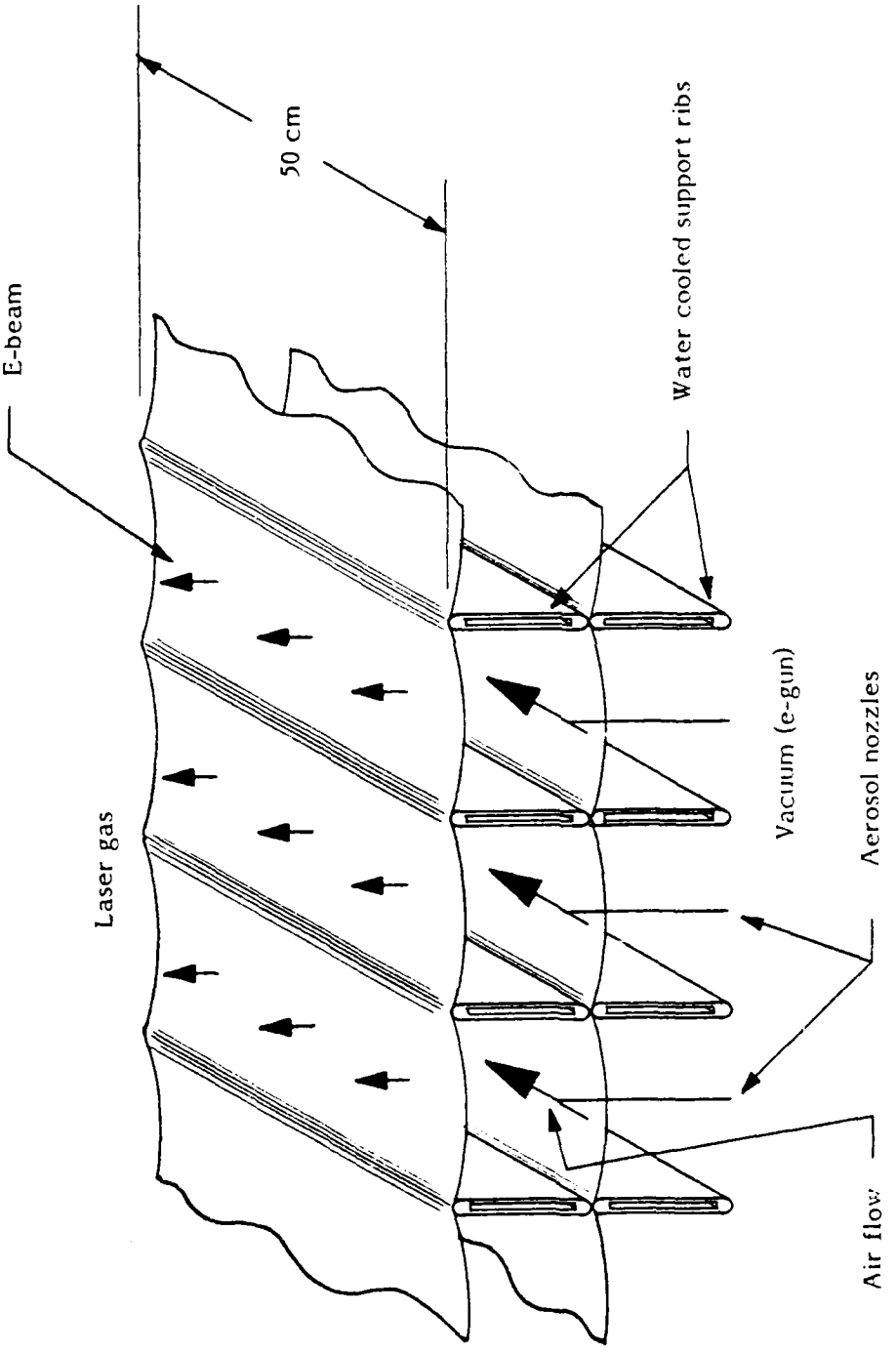

Fig. 2.3 Dual Foil Structure

a. Rib supported foil - medium (1-2 atm.) pressure in flow chamber passages

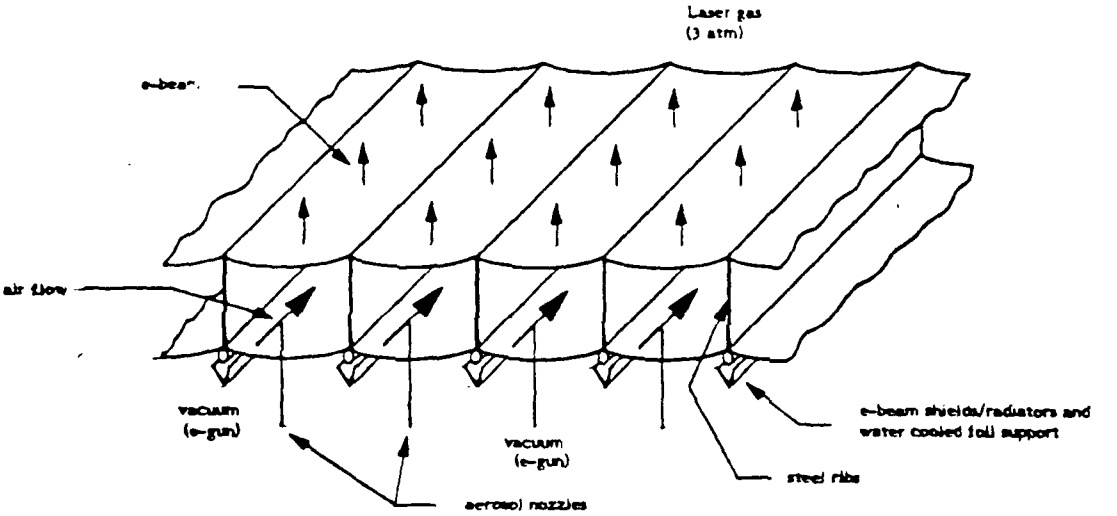

b. Tube supported foils - high pressure (greater than 3 atm.) in flow chamber

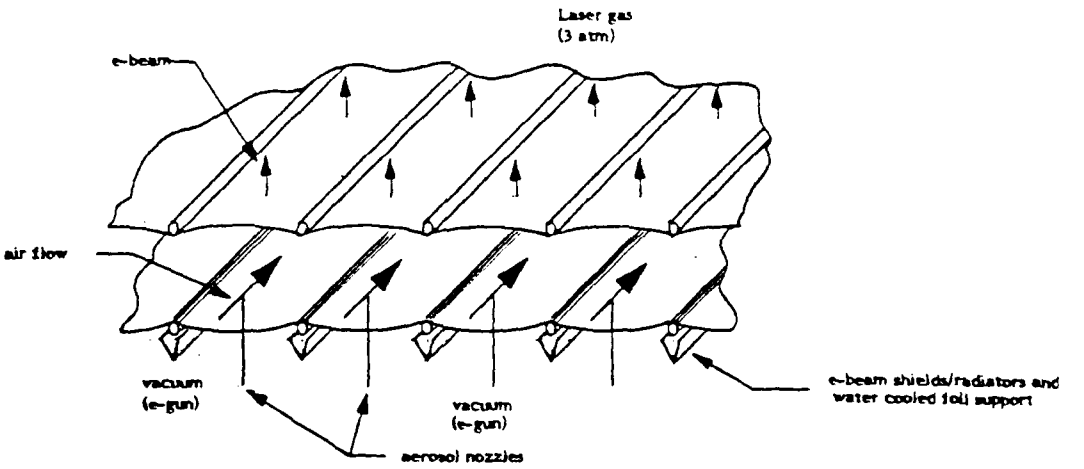

c. Tube supported foils - medium (1-2 atm.) pressure in flow chamber

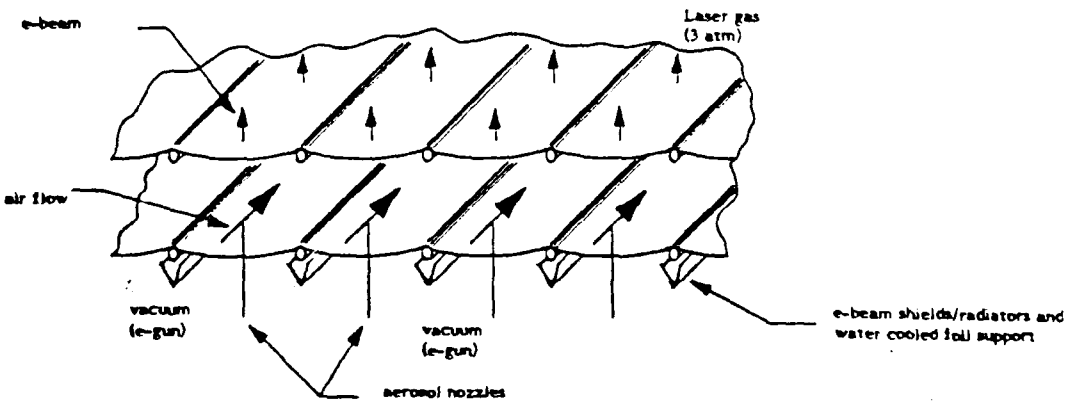

Fig. 2.4 Alternative Dual Foil Structure

not specifically addressed in this program. In extrapolating the above small area results (< 1 cm^2) to the large sizes of interest (laser window width ($\geq$ 50 cm, total area ~ 1 m^2), and to the dual foil geometries required to be compatible with the laser system, several key technical issues must be resolved. These include:

Average temperature of the foil in relation to the average temperature of the laser gas.

The pulsed thermal loading of the foil in contrast to the constant heat flux of the small scale test.

Efficiency of coolant utilization in terms of areal density presented to the electron beam for large aspect ratio structures.

These items will be discussed in the sections to follow.

2.1 Thermal Interaction

The potential thermal interaction between the laser gas and the electron beam foil presents some very unique problems for the phase transition and conductive cooled system. If the foil or its supporting structure is at a temperature significantly less than the temperature of the laser gas it is possible that a very significant heat transfer will take place from the laser gas to the foil and supporting structure. This will not only add to the heat load for the window structure but may also generate density disturbances in the laser gas that could significantly affect the laser's optical quality and efficiency.

A limitation of the conduction cooled foil is then evident. In order to provide for a large thermal transport there must be a large Δ T from the center of the foil to its perimeter support. Since foils are limited to a maximum operating temperature this implies that the perimeter of the foil will most likely be significantly less than the laser gas temperature. The phase transition cooled structure discussed previously is a face cooled geometry, therefore its temperature will be spacially uniform if the cooling is uniform.

The phase transition cooled data shown earlier indicates that the mean substrate temperature is approximately equal to the liquid's vaporization temperature. For some laser systems the ambient temperature of the gas may be 200°C. If water were used as a liquid in this situation, very significant heat loading of the e-beam window by the laser gas would be present. In order to bring the foil temperature in closer approximation to the laser gas temperature one of two things must be done. The pressure in the channel can be raised to increase the vaporization temperature of the water, or a liquid with a boiling point, at atmospheric pressure, closer to the laser gas temperature could be utilized. As is shown in Table 2.1 operating at elevated pressures will significantly increase the vaporization temperature for the water. However, to achieve the temperature in excess of 150°C the use of unreasonable high pressures in the flow channel would be required. Operating with a liquid other than water is certainly feasible and we have identified ethylene glycol as a suitable substance for these initial experiments. At atmospheric pressure its vaporization temperature is 198°C. A disadvantage to the use of ethylene glycol is its reduced heat of vaporization. It is approximately one third that of water and therefore would require three times more mass density in front of the electron beam than water requires to achieve the same amount of energy extraction.

TABLE 2.1

Vaporization Temperature of Water at Selected Pressures

Vaporization Temperature (^{o}C)	Pressure (atm absolute)
100	1
125	2.3
150	4.8
175	8.8
200	15.3
225	25.2
250	39.2

2.2 Pulsed Loads

If a constant heat load input to a dual foil structure is assumed and stable temperature operation is achieved, there will necessarily be an excess of water in the flow stream as was described earlier. Some of this excess water will wet the surface with a thin film whose thickness would be determined by the air velocity, the fluid viscosity and the surface treatment of the foil. The heat flux into the foil will then determine the rate at which water is vaporized from this film by the substrate. For a pulse loading situation, where the heating of the foil is timewise divided into discreet packets of energy, the situation would be considerably different. For example, if the energy is divided into pulses two microseconds wide, separated in time by 10 milliseconds, the following situation would probably occur. After equilibrium is achieved, and the foil has been reduced in temperature to slightly less than the vaporization temperature of the liquid, a thin water film would form on the foil surface. At the time of the next pulse the foil will experience a heating rate of approximately 500 kilowatts per square centimeter. At this rate of power delivery , the thin film of water on the surface will quickly vaporize leaving the foil surface dry. During the next 10 millisecond period, before another pulse arrives, additional liquid must come in contact with the foil surface in order to promote the additional vaporization required to return the foil to the vaporization temperature. The situation will likely lead to a two rate cooling equation. In Fig. 2.5 we have illustrated what the instantaneous temperature of the foil may look like. There is of course a trade off between the amount of energy extracted during this first instantaneous drop of temperature and the amount of energy extracted during the slower decay time where the aerosol stream is actively participating in the cooling.

It is possible to consider a situation where all the cooling occurs in the first instantaneous drop. For example, for a heat of vaporization of 2 kJ per gram, and to cool at a rate of 100 watts per square

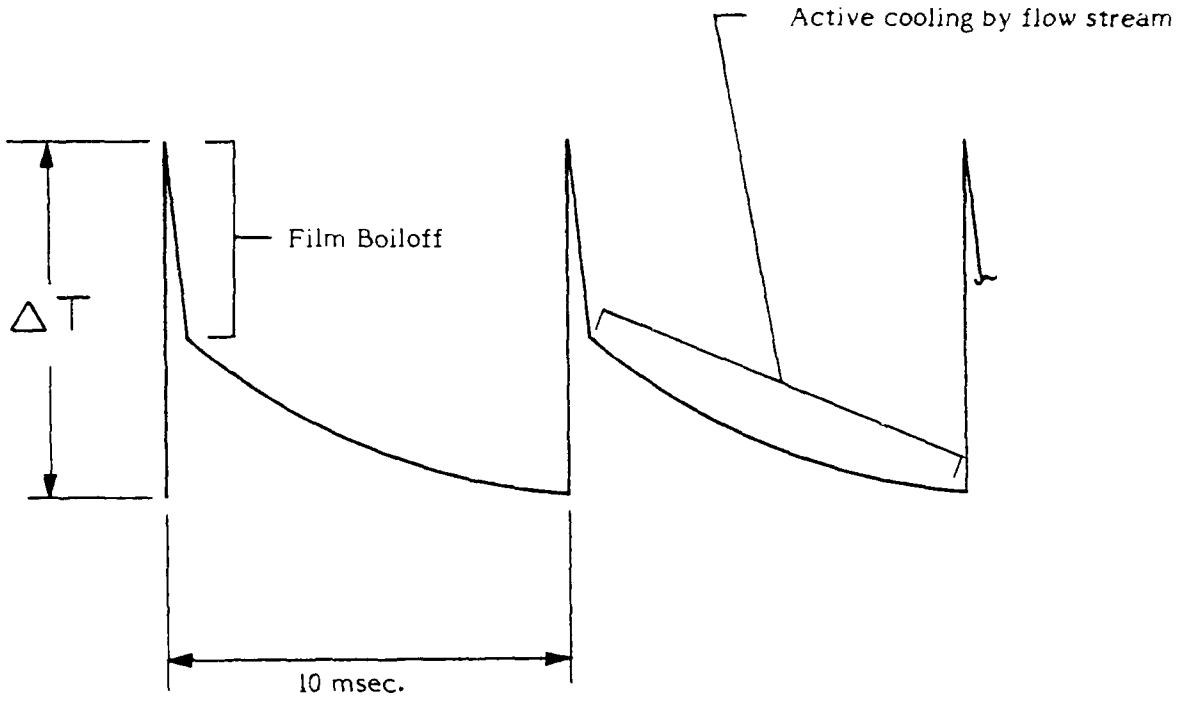

Fig. 2.5 Cooling of Pulse Heated Foils

centimeter per foil, at a pulse rep rate of 100 pps, the energy we must extract on any one pulse is 1 joule per square centimeter. The thickness of liquid that must be deposited on the foil surface between pulses in order to remove one joule per square centimeter is 0.5×10^{-3} cm or, an areal density of 0.5 milligrams per square centimeter.

2.3 Efficiency

The efficiency of phase transition cooling is an important system consideration. An aspect of this consideration is the additional areal density that the aerosol flow presents to the electron beam. The amount of liquid used in the cooling process is insignificant in any system application and is not a prime consideration. The amount of mass density presented to the electron beam is determined by the following equation:

$$\text{Areal density} = \frac{1}{\eta \lambda} \left[\frac{\phi \ell}{v} \right]$$

Where

η	efficiency of utilization
ℓ	length of flow dimension
v	flow velocity
λ	heat of vaporization
ϕ	power density

As is apparent, the efficiency directly enters into the expression for areal density. The efficiency of utilization is directly related to the effectiveness with which the liquid can come in contact with the foils. Very poor efficiencies can result for those structures with a high aspect ratio, that is a channel length to heigth ratio greater than or equal to ten, if sufficient turbulence is not generated in the flow channel.

SECTION 3

EXPERIMENTAL APPARATUS AND TECHNIQUES

This section describes the experimental apparatus and the techniques used to obtain the data for this project. The discussion is divided into two major sections. The first section describes the experimental apparatus that was used to simulate the laser window and the thermal loading conditions that high average power laser window foils would encounter. The second major section describes the actual laser window that was tested under repetitive pulse e-beam gun operation.

3.1 The Simulation Test Cell

The purpose of the simulation test cell was to demonstrate the heat transfer capabilities of phase transition cooling, and to measure the basic parameters. These parameters included the heat transfer film coefficient as a function of aerosol ratio, aerosol flow rate, aerosol utilization factors, and uniformity of the foil temperature distribution. After the phase transition cooling was demonstrated, the actual laser window was constructed and tested under e-beam loading of the window foils. This laser test cell was consistent with high average power laser geometries.

Two possible methods were envisioned to simulate the laser window and the thermal loading conditions of the foils. One was to heat a foil and support structure using incandescent lamps, and the second was to embed cartridge heaters in a massive copper block, and employ a thin stainless steel overlay brazed to the copper, to simulate the foil. Phase transitition cooling would then be demonstrated in either case by passing an aerosol mixture over the heated foil, thus cooling it. The latter method was chosen to demonstrate the large heat removal capabilities of phase transition cooling.

The simulation test cell featured flexibility in its assembly configuration. Modular units were constructed of copper with a thin stainless steel overlay brazed to the top surface to simulate the window foil as mentioned previously. Resistive cartridge heaters were embedded in the copper to provide a regulated heat source to simulate the thermal loading conditions of the actual window foils. Each of the modular units was 6.4 cm high x 15 cm wide x 12.5 cm long. By adjoining the copper block units adjacent to one another, the desired length of the aerosol flow channel was achieved. This flow channel, where the cooling aerosol passed over the simulated foil (that is, the stainless steel overlay) measured 5 cm x 1 cm in cross section and up to 50 cm in length. Each of the modular units added 12.5 cm to the length of the aerosol flow channel. Glass panels, .6 cm wide x 1 cm high x 12.5 cm long, placed 5 cm apart on top of the stainless steel overlay, formed the sides of the aerosol flow channel. The aerosol was injected parallel to the 12.5 cm dimension. In the initial testing, the bottom of the flow channel was the stainless steel overlay while the top was a glass panel or a thin Kapton film. One of the modular units is shown in Fig. 3.1 without the glass side panels which make up part of the flow channel. The thin stainless steel overlay is seen in this figure brazed to the copper block. Thermocouples are shown attached to the stainless steel along the flow channel. Also, two small holes used as optical access ports for the laser scattering diagnostics are shown in the center of the flow channel.

Fig. 3.2 is a representation of the simulation test cell and shows the components which make it up. Initial testing was done with this configuration with four units as shown in Fig. 3.2, but final testing of the simulation test cell was done with another full length, 50 cm test cell stacked on the top of the flow channel. This configuration simulated a foil on each side of the flow channel, through which the air/aerosol mixture was injected. Stacking the test cells delivered symmetrical heat input to the foils. Actual laser windows will be constructed this way and the electron beam will deposit energy in both foils. Therefore, testing with the stacked configuration yielded more realistic data than testing with blocks present on

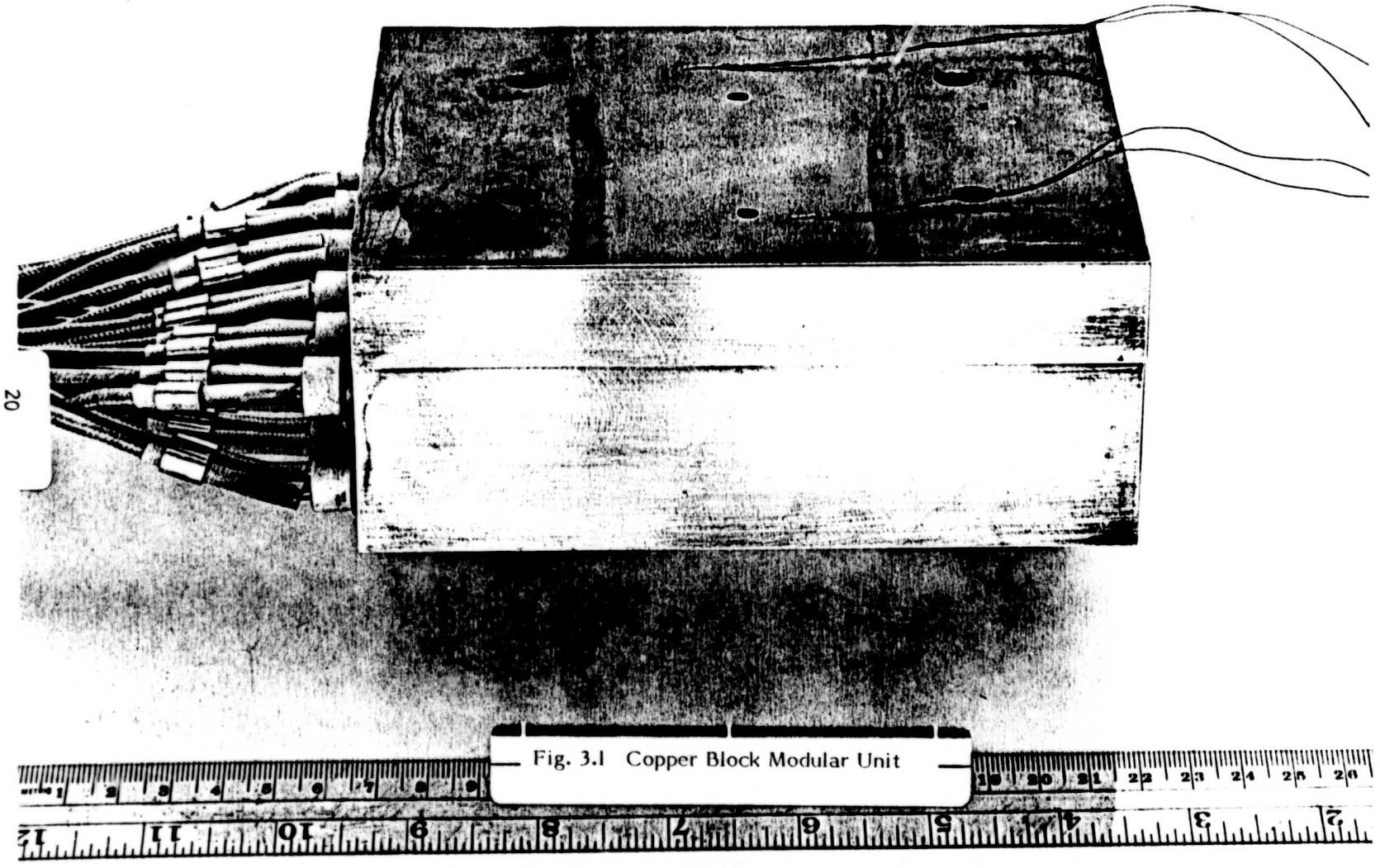

Fig. 3.1 Copper Block Modular Unit

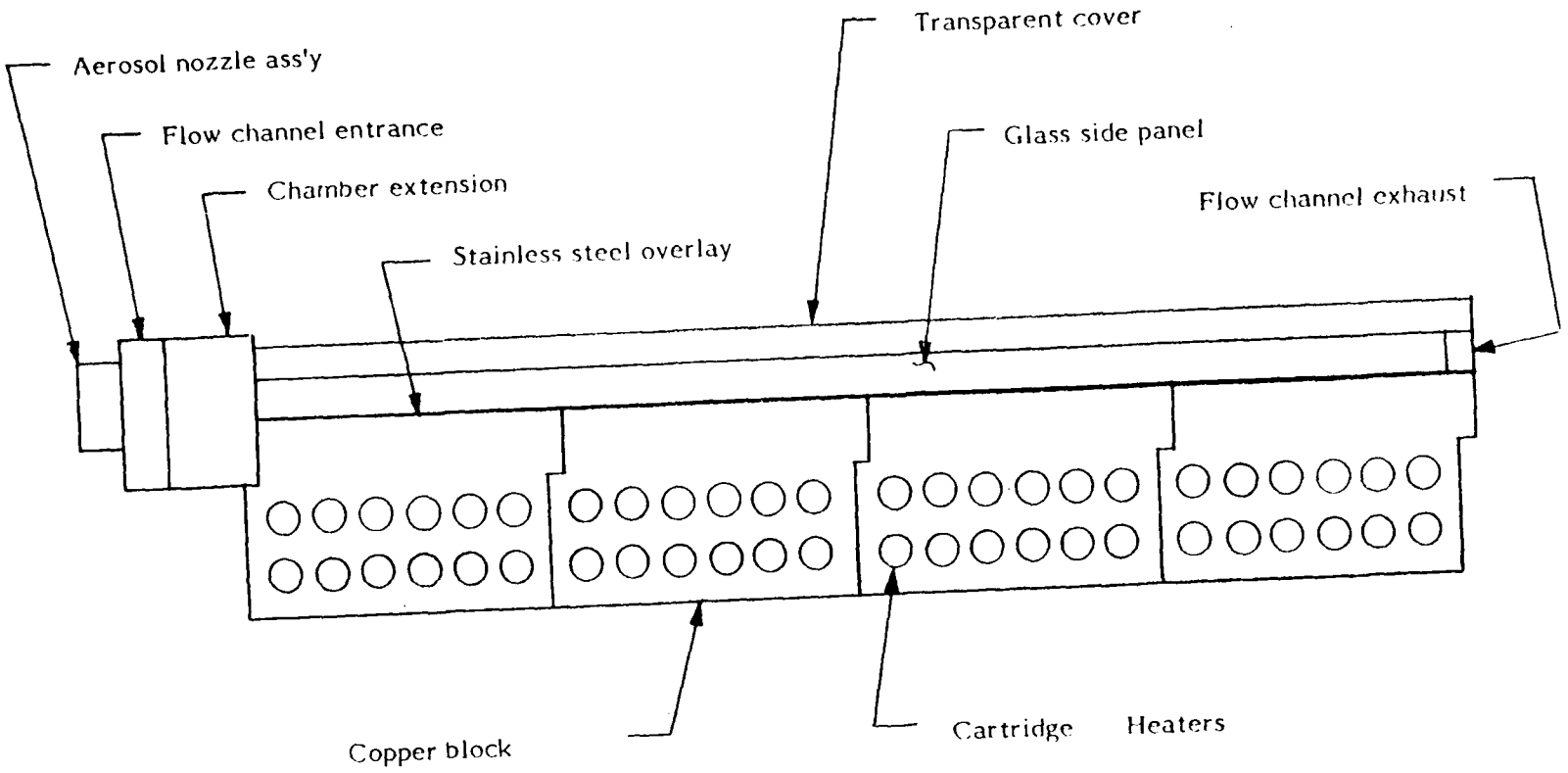

Fig. 3.2 Representation of Full Length Simulation Test Cell

only one side of the channel. Fig. 3.3 shows the stacked configuration, with blocks on the bottom of the flow channel, which were used in the final testing of the simulation test cells.

The regulated heat source was required to deliver up to 350 W/cm^2 or 87.5 kw of total power to a 5 x 50 cm^2 surface. It was determined that the most straightforward method to accomplish this was to utilize resistive cartridge heating elements. Maximum output per element, for a size compatible with the test cell dimensions, was $\sim$ 2100 w. The use of 48 elements per test cell provided up to 100 kw of available power. There were twelve elements per block with two rows of six each, imbedded in the copper, to attain maximum heat transfer to the lower surface of the flow channel. As a result of the power loading required, the ΔT in the copper was designed to be 600°C. Similarly, the ΔT in the stainless steel overlay was designed to be 100°C.

Regulation of the heat source was performed by controlling the current to the heater cartridges. An SCR current control unit operating from 208 Vac, 3 ¢ input provided the control. The SCR controller is shown in Fig. 3.4. The current transformers which monitored the cartridge heater current are shown mounted on the panel near the top of the cabinet.

As mentioned before, in this test cell design the window foil was simulated by a thin (0.6mm) stainless steel overlay brazed to the copper blocks. Stainless steel has a low thermal conductivity ($k_{copper}/k_{stainless} \simeq 28$) and thus the heat transfer in the foil by thermal conduction was minimal compared to the heat transferred to the aerosol. This is shown in Fig. 3.5 and explained in the following discussion:

We have $\left(\frac{Q}{t}\right)_v = -kA_v \left(\frac{\Delta T}{L}\right)_v$, and $\left(\frac{Q}{t}\right)_h = -kA_h \left(\frac{\Delta T}{L}\right)_h$

(See Fig. 3.5 for definition of symbols)

We desire the heat transfer to be ten times greater in the vertical direction than in the horizontal direction, i.e.

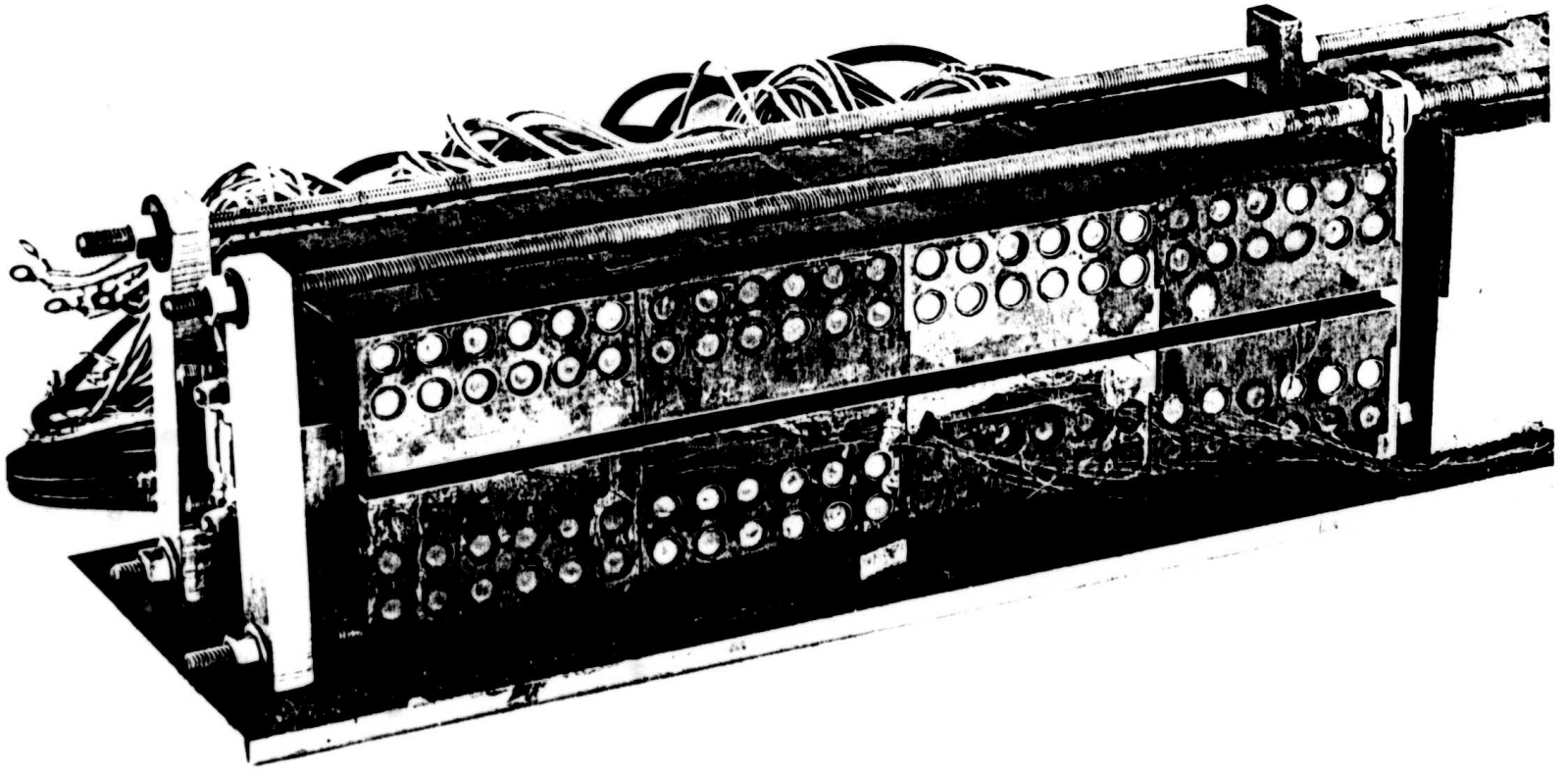

Fig. 3.3 Simulation Test Cells in Stacked Configuration

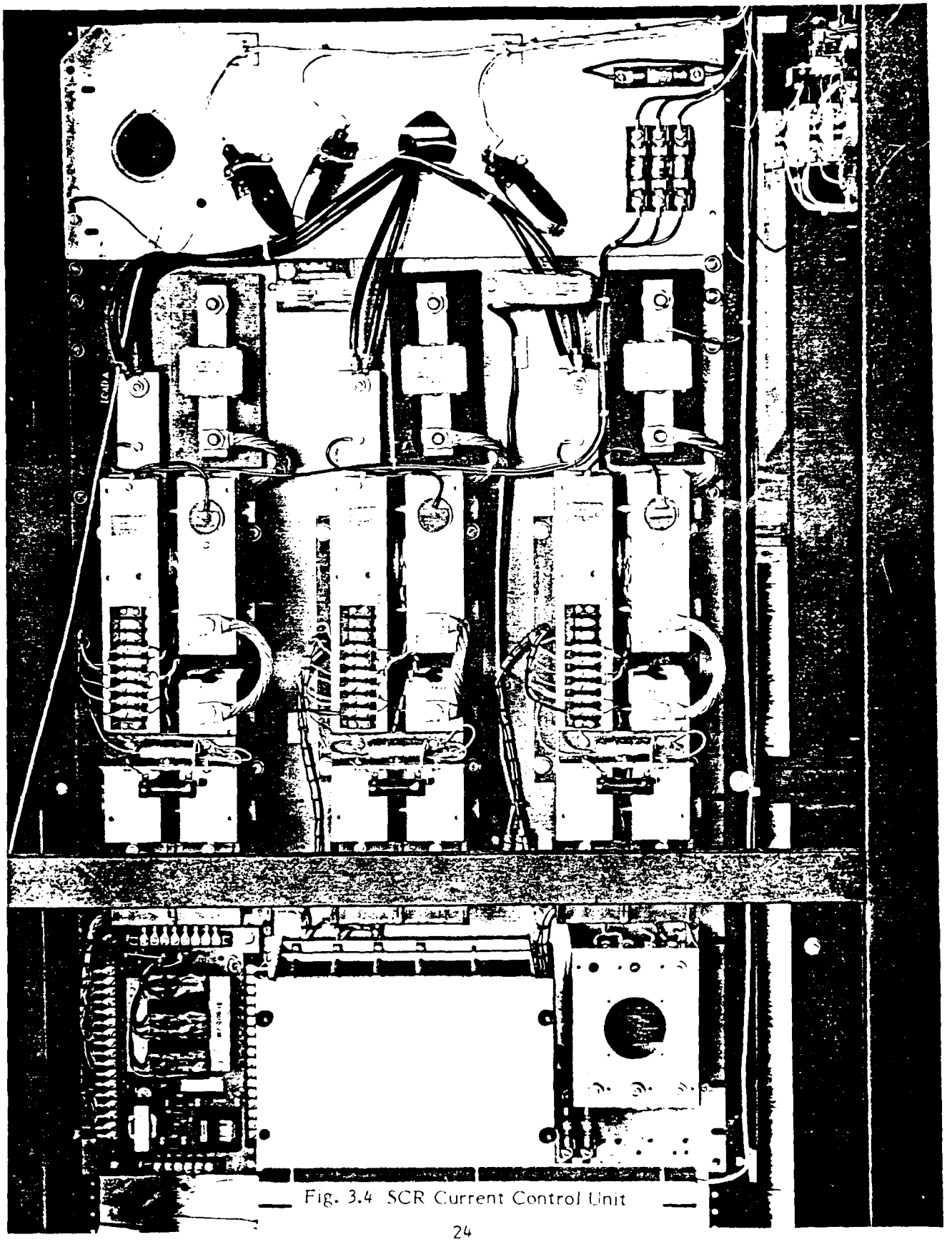

Fig. 3.4 SCR Current Control Unit

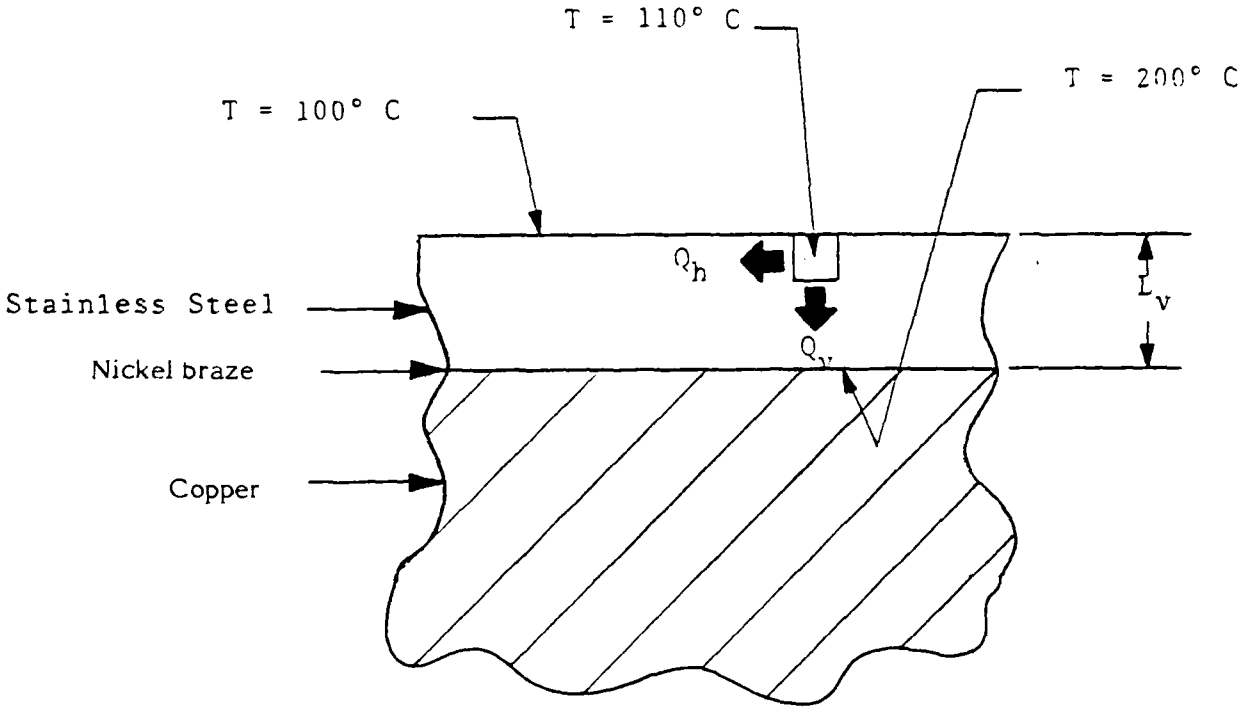

Definitions:

h, v	subscripts denoting quantities relating to heat flow in horizontal (h) or vertical (v) directions
Q	quantity of heat
A	area through which heat flows
k	thermal conductivity
L	dimension in direction of heat flow
T	temperature
t	time

Fig. 3.5 Heat Flow in Stainless Steel Overlay

$$\left(\frac{Q}{t}\right)_v = 10\left(\frac{Q}{t}\right)_h \quad , \quad \text{and if } A_v \simeq A_h, \text{ then } \left(\frac{\Delta T}{L}\right)_v = 10\left(\frac{\Delta T}{L}_h\right)$$

This gives the $\Delta T_v = 90^{\circ}C$ and $\Delta T_h = 10^{\circ}C$, and $L_v = 0.6$ mm. Solving for L_h yields ~ 0.7 mm. The braze material was mostly nickel and was only 1 mil thick. The calculated ΔT across the braze was about $1^{\circ}C$ and therefore was negligible. Besides the minimal lateral heat transfer in the stainless steel, another important feature is brought out here. This design yields a $10^{\circ}C$ lateral temperature resolution. This is important because the foil temperature distribution along the channel was one of the parameters that was to be determined, and this $10^{\circ}C$ resolution allowed for a detection by the infrared diagnostics of any "hot spots" that would develop as a result of insufficient cooling by the aerosol.

At this point the importance of the brazing between the stainless steel overlay and the copper blocks can be seen. If the brazing is not uniform, or there are some flux inclusions or cavities, the thermal contact is poor and the heat transfer would be hindered. These areas, or spots, would then appear in the foil as either cool or hot areas in comparison to the adjacent area. The first block was in fact inadequately brazed and the heat transfer characteristics were severely hindered. The brazing techniques were modified until 100 percent bonding was accomplished in the later blocks.

The nozzles used to mix the air and liquid were manufactured by Spraying Systems Co. as a standard catalogue item. They were internal mixing, atomizing, nozzles with interchangeable air and fluid caps. Three different spray patterns were available.

Spray Set Up No.	Fluid cap No. Air cap No.	Spray Pattern
J22	J60100 J1401110	full cone, round spray
J23	J60100 J125328	flat spray
J29	J60100 J140-6-52-70°	wide angle round

To insure that the aerosol from the nozzles mixed optimumly, up to 15 cm of drift space could be inserted at the entrance of the flow channel. Also from one to four nozzles could be inserted at the entrance of the flow channel. During the course of testing, all of the nozzles were used in various combinations and geometries to maximize efficiency of the system and minimize areal density. Fig. 3.6 shows a two nozzle assembly that was used in testing. The slot in the mixing chamber had the same cross sectional area as the flow channel. Part of the air and water connections are shown above and below the mixing chamber.

The nozzles produced a very fine, atomized aerosol with an average droplet size of 35 μm. The aerosol was injected into the entrance of the flow channel, and the steam and unconverted aerosol were exhausted to the atmosphere out the other end of the channel. The other cooling liquid that was used, ethylene glycol, was not as readily exhausted. Attempts were made to condense the exhausted glycol aerosol vapors by passing them through a heat exchanger and then through a "scrubbing" stack. The purpose of the stack was also to condense, or "scrub", the glycol vapor using water droplets as a condensing medium.

The liquid and air were supplied to the nozzles by the supply system that is shown in the schematic in Fig. 3.7. This system was used throughout the program and was designed for operation with water or glycol or other cooling liquids. The air flow system consisted of a high volume air compressor, air flow meters, a pressure regulator, flow valves and associated piping. The liquid flow system likewise included flow meters, a pressure regulator, flow valves and necessary plumbing. Liquids other than water could have been used in the system by filling a 30 gallon tank and pressurizing it. This is how the glycol was supplied to the delivery system.

During the initial testing of the simulation test cell, problems were encountered when regular tap water was used as a coolant. Scale buildup on the channel surface offered a significant impedance to the heat flux. This strongly interfered with the cooling process. The addition of a

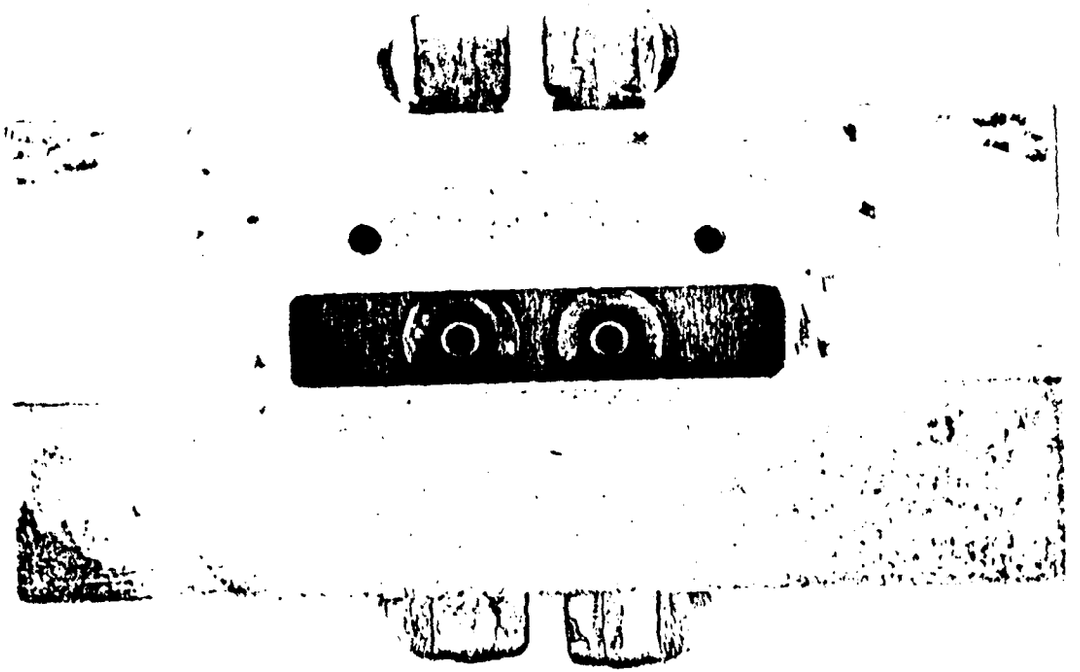

Fig. 3.6 Two Nozzle Assembly

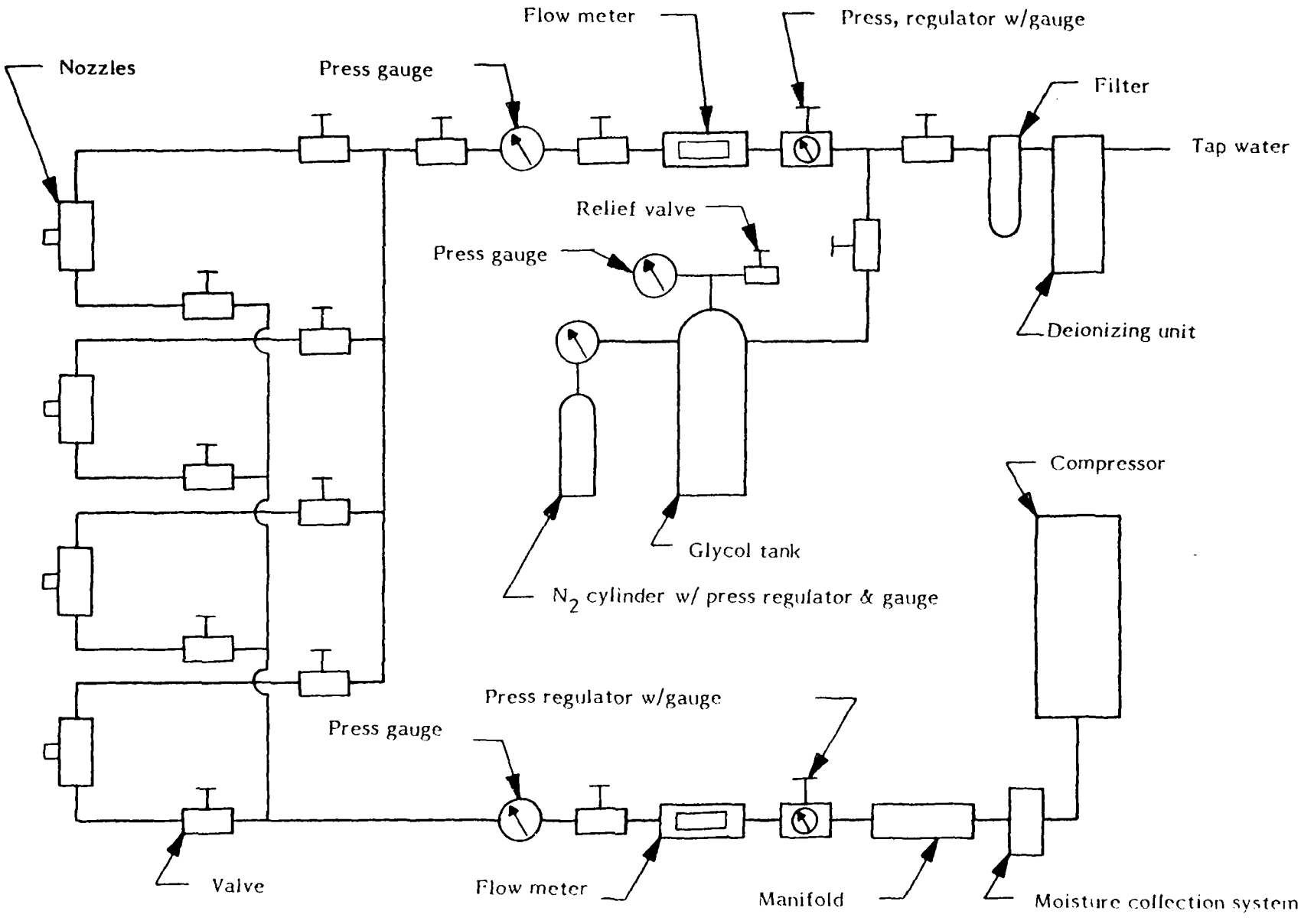

Fig. 3.7 Schematic of Air and Water/Liquid Supply System

deionizing unit to the supply system eliminated this problem and allowed many hours of operation without any significant scale buildup. This is important since long run times are required (30 min) in order to provide for stable readings.

Measurements of the basic parameters of the test cell to evaluate heat transfer efficiency and transparency of the system to an electron beam required determining the aerosol ratio, aerosol flow rate, aerosol utilization factor, heat input to the simulated foil, and foil surface temperature distribution. Thus diagnostics and diagnostic access were important in the design of the simulation test cell.

The aerosol ratio is the volume of liquid to air. It was determined by measuring the volumes of air and liquid flowing through the injection nozzles. This information was obtained from the pressure gauge and flow meters in the aerosol injection system. Measurement of the aerosol ratio at different locations in the flow channel required the use of more sophisticated techniques such as the measurement of laser light scattered by the aerosol.

The initial aerosol flow rate is the rate at which aerosol is injected into the flow channel. This information was also obtained from the diagnostics in the aerosol injection system. The aerosol flow velocity (a short distance away from the nozzles) was calculated from the initial flow rate and the channel dimensions. The aerosol utilization factor is the percentage of the liquid component of the aerosol which is converted to vapor; this is related closely to the efficiency of the system. This factor was determined for the system by measuring the power input into the heaters and the volume of water/liquid which was injected into the flow channel.

The power input into the heaters was measured through the use of current and voltage meters at the SCR Controller. The volume of water/liquid was obtained from the flow meters in the aerosol injection system. To determine this factor at specific channel locations, the scattered laser light measurement was required.

The laser light scattering technique operates on the principle that the HeNe beam scatters off the surface of the water droplets, but will pass through the water vapor undisturbed; the amount of scattered light is then directly proportional to the aerosol concentration.

This measurement was accomplished in our system by passing the beam through the flow channel transverse to the direction of flow, and detecting the scattered light with a photomultiplier tube via a fiber optic probe. The fiber optic probe was inserted through the holes drilled in the upper blocks with the end of the probe even with the flow channel surface.

This probe became necessary because of the loss of the optical access port when the test cells were tested in the stacked configuration as mentioned earlier. The unwanted light was filtered out. Fig. 3.8 is a schematic showing how the laser scattering measurements were made.

The surface temperature distribution over the entire channel area could not be determined precisely as a result of three factors. Two of these factors occurred while testing with a single 50 cm full length test cell, using one mil Kapton as the optical window (Kapton was used because of its mechanical and thermal properties, and its transmission capabilities in the infrared).

The first factor was the absorbent paint (3M Corp. Nextel) used to treat the foil, or the stainless steel overlay, to enhance its emissivity. The heat transfer characteristics were significantly changed as a result of this treatment being applied to the surface of the flow channel (thermal conductivity of the Nextel was close to that of carbon $\sim .018\ W/cm^2$), and thus the correct surface temperature could not be obtained. This treatment was necessary in order to obtain a meaningful temperature measurement of the foil, because of the high reflectivity and low emissivity ($\simeq 0.05$) of the stainless steel. Fig. 3.9 shows the heat transfer characteristics with and without the treatment.

The second factor was due to the absorption of infrared by the water aerosol in the critical bandwidth (3.2 - 20 μ) of the thermal scanner. As a result, the thermal scanner yielded no meaningful temperature measurement. Fig. 3.10 compares the infrared bandwidth of the thermal scanner with the absorption of infrared by water in the same bandwidth.

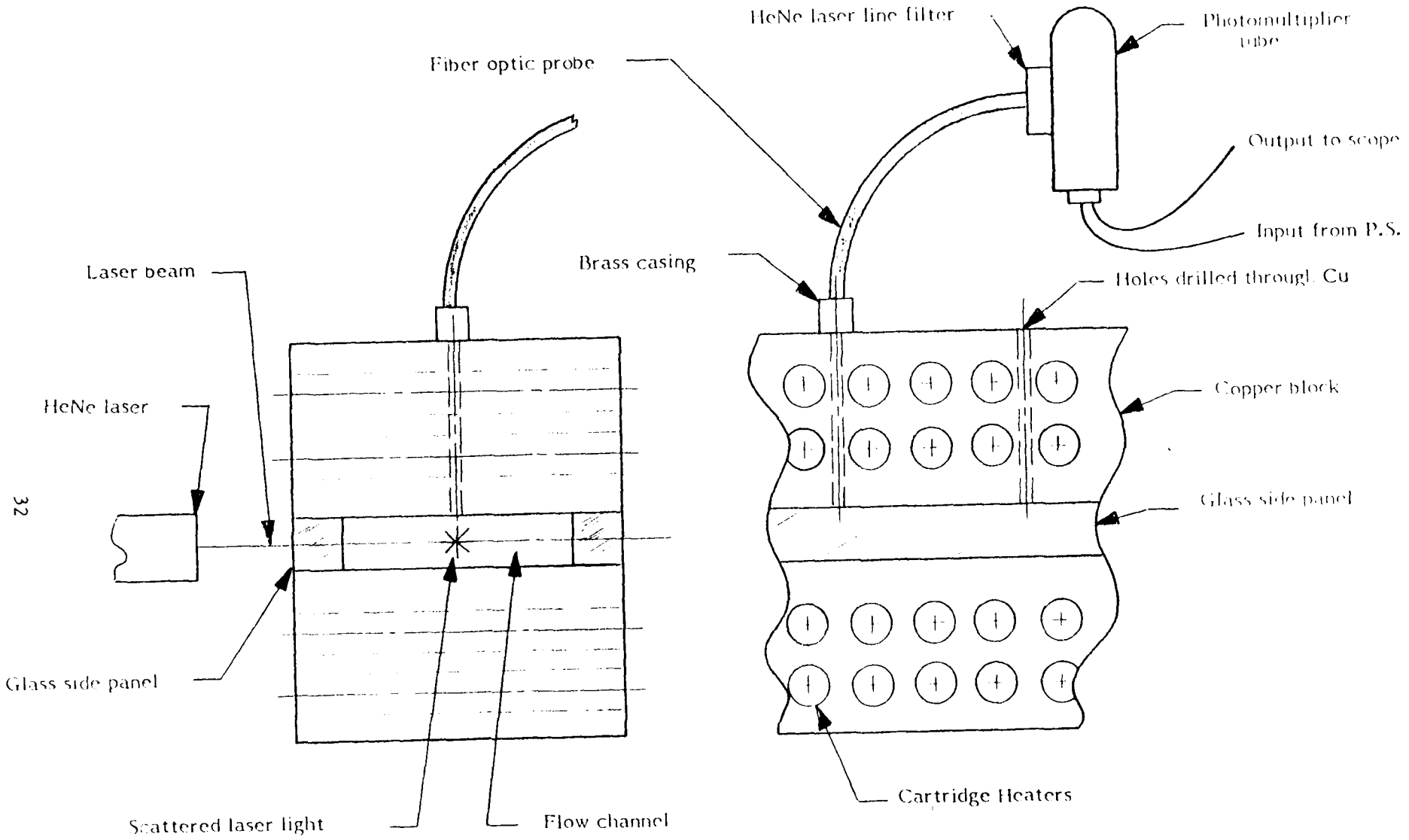

Fig. 3.8 Schematic of Laser Light Scattering Diagnostic

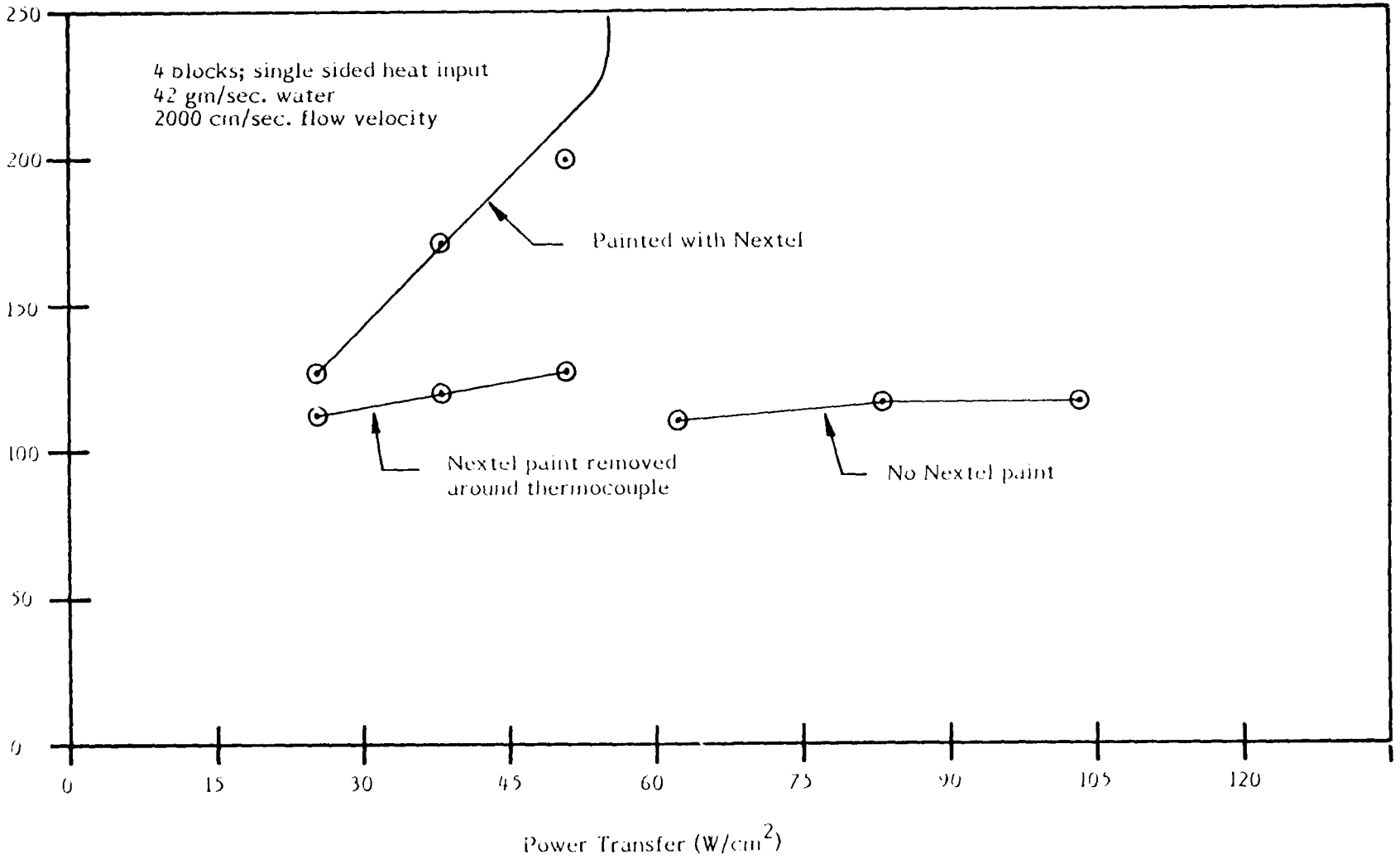

Fig. 3.9 Heat Transfer Characteristics

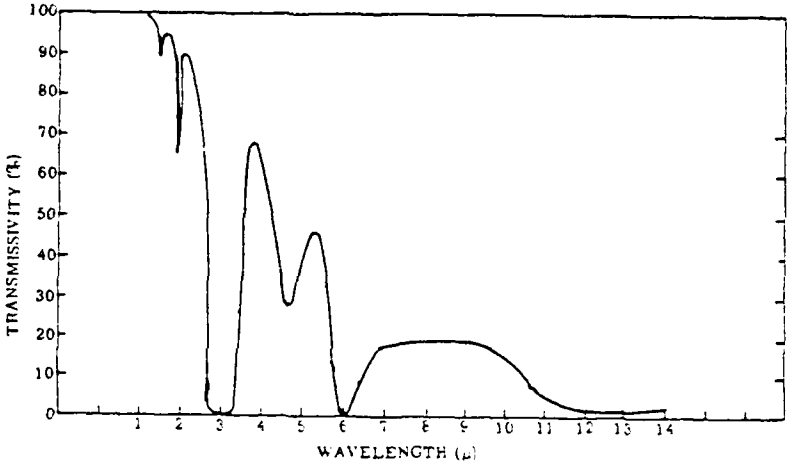

Absorption by water

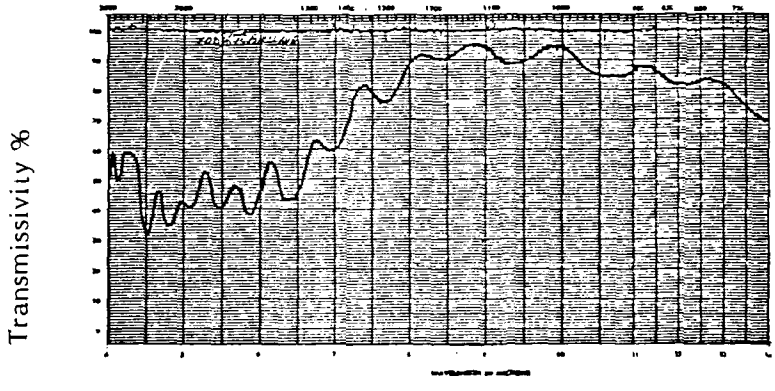

Infrared bandwidth detected by thermal scanner

Fig. 3.10 Infrared bandwidth detected by scanner and absorption by water in the critical bandwidth

The third factor occurred because of stacking the simulation test cells on top and bottom of the flow channel. By eliminating the optical access port the channel surface could no longer be viewed with the thermal scanner. However, the surface temperature distribution was determined at specific locations along the length of the flow channels using chromel-constantan thermocouples spot welded to the foil surface. Two thermocouples were used per block so that an array of thermocouples yielded the surface temperature information of both foils along the length of the channel. To insure that the aerosol flow would not be impeded, ten mil thermocouple wires were used.

The purpose for measuring the temperature distribution over the entire channel area was to determine if any "hot spots" developed due to inadequate aerosol flow. It was found that the instabilities that did develop spread quickly to the surrounding areas, which were then detected by the thermocouples.

3.2 Laser Test Cell

After successfully demonstrating the large heat removal capabilities of the phase transition cooling technique with the simulation test cell, an actual laser test cell was designed and constructed. Information obtained from the simulation test cells in the stacked configuration was used to help guide the design of the laser test cell. The purpose of the laser test cell was to evaluate the performance of phase transition cooling under actual e-beam thermal loading of the window foils using a geometry consistent with high average power laser requirements. Properties that were investigated included window survival, foil temperature distribution, fatigue limits, and potential corrosion problems.

The laser test cell was designed to be compatible with the GFE S-Cubed/BMD spark cathode gun test chamber. The test cell consisted of the window plate, cooling cavity, window clamp, gas chamber, and blank-off plate. Fig. 3.11 is an exploded view showing how these components assembled. The test cell mounted on the outside of the spark cathode test chamber end plate which also served as the window plate for the laser test

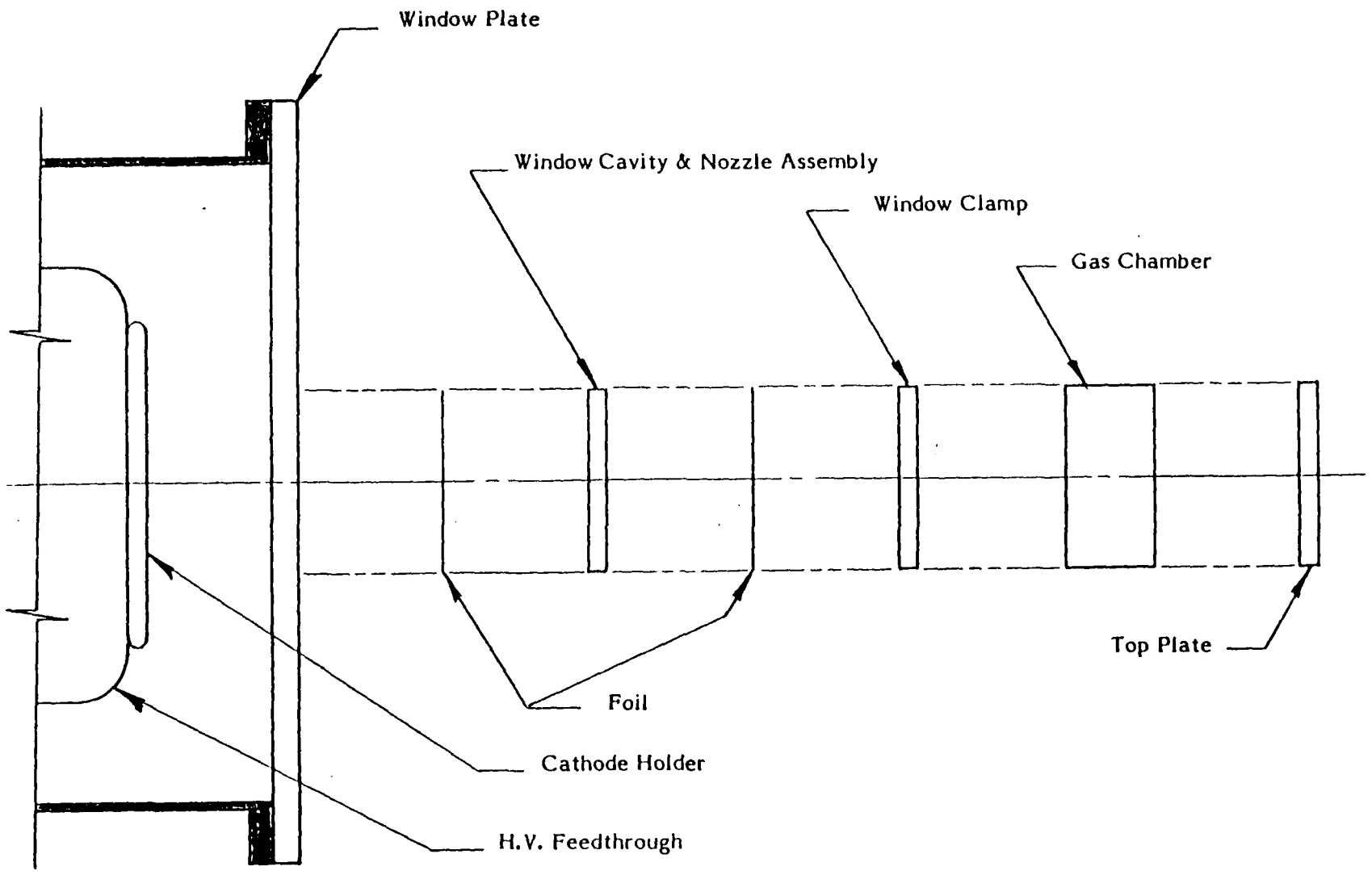

Fig. 3.11 Laser Test Cell Assembly

cell. The window plate had two parallel slots cut out of the center in line with the cathode, so that the electron beam could be transmitted into the window assembly. Between the two horizontal slots there was a rib which provided support for the foil that was mounted on the outside of the window plate. A photograph of the window plate is shown in Fig. 3.12. This first foil terminated the test cell cavity at the gun end and sealed the high vacuum side from atmospheric pressure on the cavity side. The e-beam passed through this foil and the second foil, into the gas chamber where the laser gas resided. On top of this first foil the cooling cavity was mounted. This cavity consisted of a 5 in. x 10 in. plate with a 3 in. x 8 in. rectangle cut out of the center which gave it an annular shape. Holes were bored through each end to allow the aerosol to be injected in one end and exhausted out the other end. Also, a 1/16 in. diameter wire was stretched across the top of this cavity to provide support for the second foil along the center line. The second foil was mounted on top of this cavity so that the cavity was sandwiched between the two foils. A clamp, with the same shape and dimensions as the cooling cavity, bolted on top of the cavity and held the second foil in place. The gas chamber mounted on top of the clamp. It had the same dimensions as the clamp except that it was 2.5 in. deep. A blank-off plate sealed off the open face so that it could be pressurized to three atmospheres of gas. Figure 3.13 is a photograph of the laser test cell showing each of the components except the window plate. The rubber gaskets which sealed the cooling cavity from leaking water/liquid are shown on each side of the cavity. Also the aerosol exhaust tubes are seen extending out from the cooling cavity.

The laser test cell was mounted on the GFE S-Cubed/BMD facility (this facility was used to develop the spark cathode under an earlier contract). This facility, which consisted of a high voltage power supply and electron gun, provided the electron beam for the laser test cell. Fig. 3.14 is a block diagram showing the major electrical components of the facility which were: a high voltage dc power supply, the charging system, the pulse forming network (PFN), the triggered output switch gap, the triggering circuit, the pulse transformer, and the electron gun. The pulse transformer

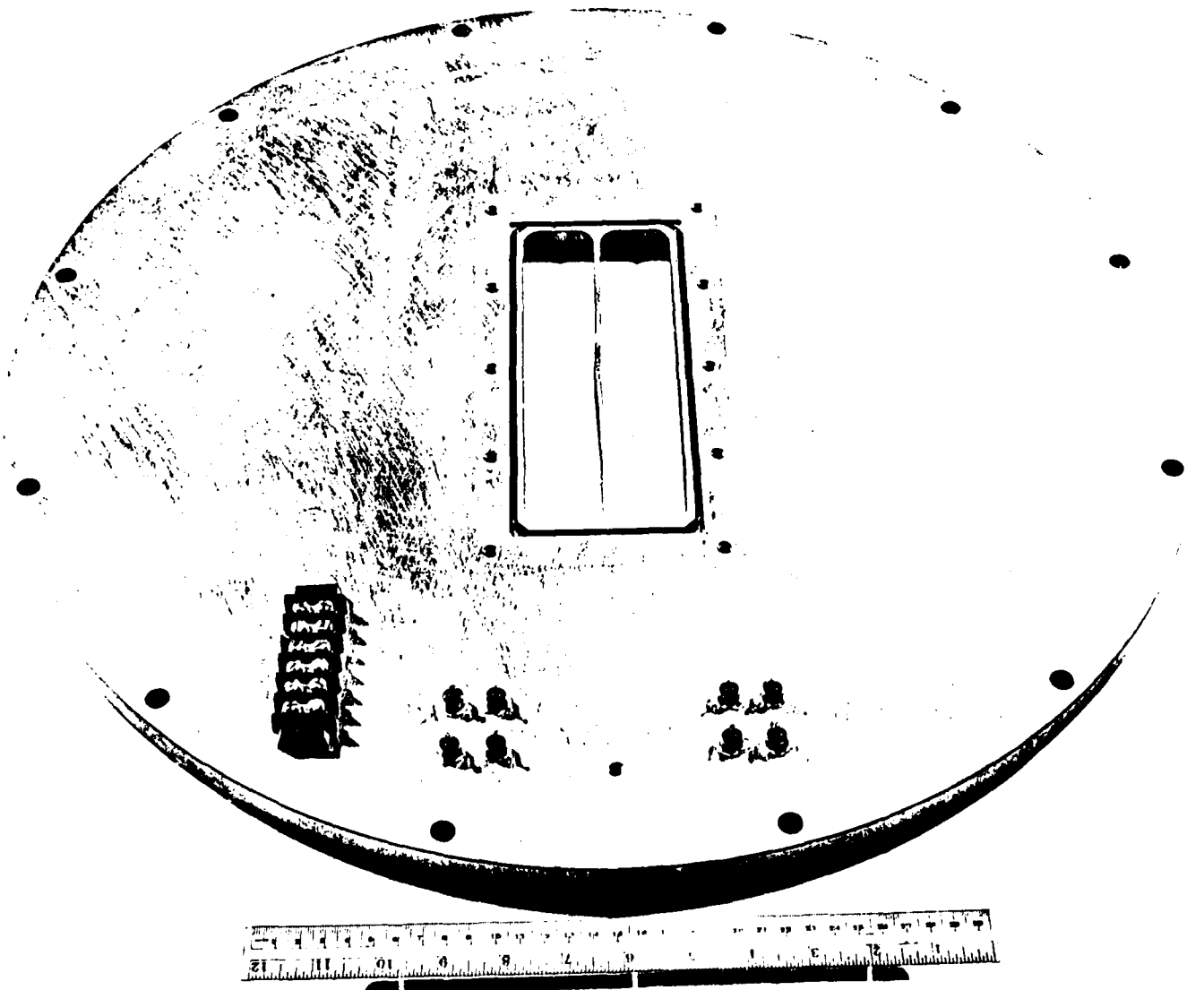

Fig. 3.12 Window Plate for Laser Test Cell

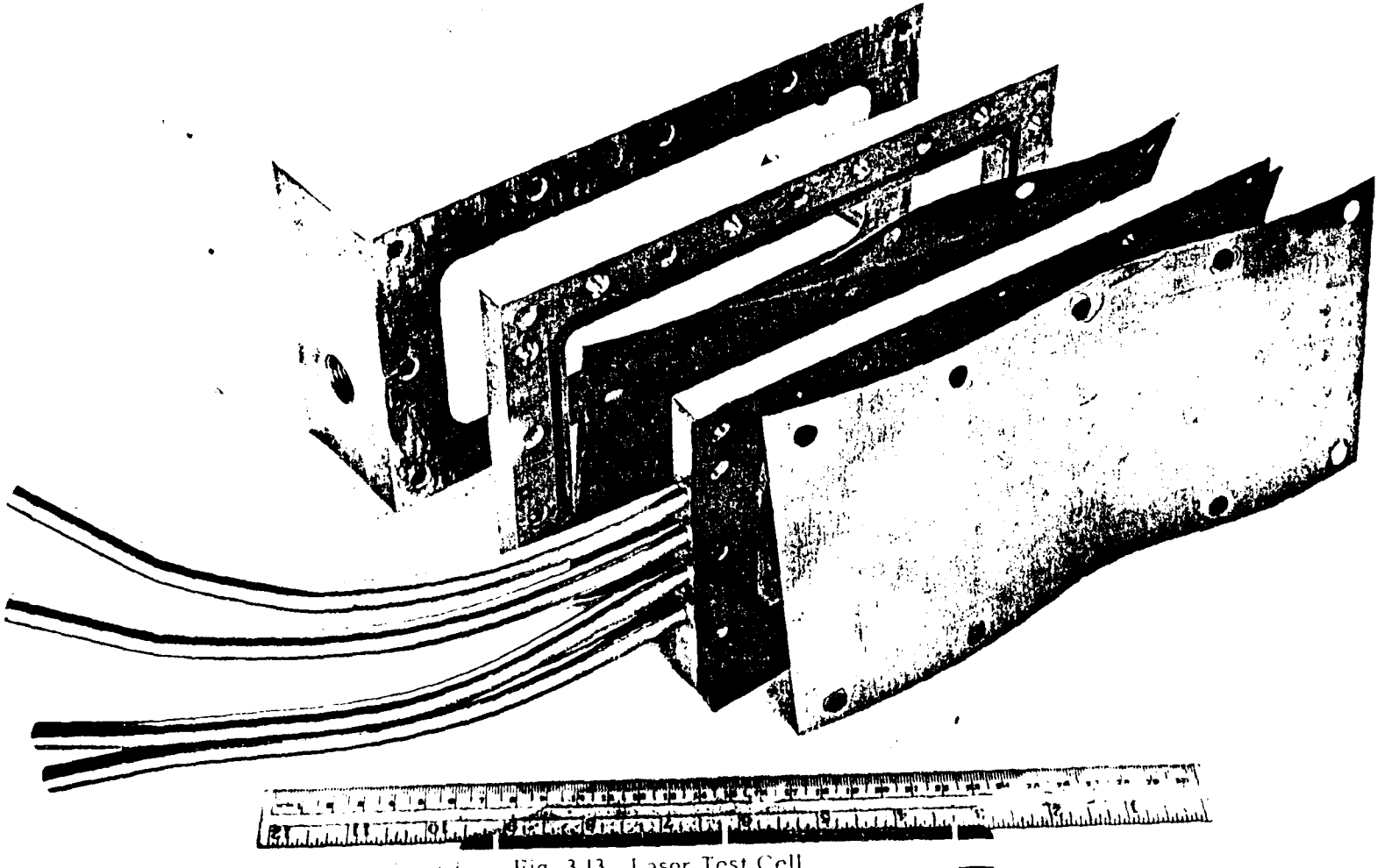

Fig. 3.13 Laser Test Cell

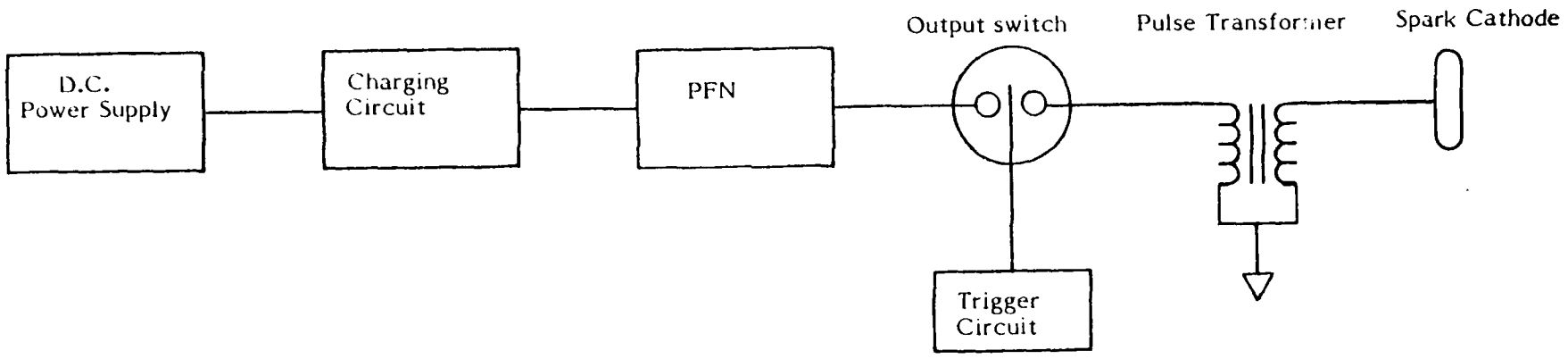

Fig. 3.14 Block Diagram of Gun Circuit

and part of the high voltage feedthrough are in the oil tank filled with transformer oil. To accommodate the laser test cell and comply with the electron beam current density requirements, some components of the spark cathode facility had to be modified; the output switch gap, the high voltage feedthrough assembly, and the cathode assembly. The output switch was modified to deliver the necessary power at a repetition rate up to 100 Hz. Also the high voltage feedthrough was lengthened. Several different spark cathodes were fabricated, which provided the option of using either a 26 cm^2 board or a 77 cm^2 board to achieve the 1 - 10 mA average beam current that was required. Both cathodes had 16 electron emission sites/cm^2 which provided the capability of depositing a uniform beam of up to 350 w/cm^2 to the foils. A magnetic field was used to focus the beam onto the 7.5 cm x 20 cm window. Fig. 3.15 is a schematic showing the cross section of the gun test chamber with the laser test cell mounted to it. Fig. 3.16 is a photograph of the test chamber with the window plate removed. Inside the test chamber the corona shield and the spark cathode are shown mounted in place. The field coil is seen around the test chamber. Directly adjacent to the test chamber, part of the oil tank is shown.

Fig. 3.17 shows the test chamber with the laser test cell mounted to the window plate. The air and water lines to the nozzles are shown in place. The photograph in Fig. 3.18 shows the 26 cm^2 cathode holder with a spark cathode mounted to it. The radius was necessary on the edges because the cathode holder was at high voltage. Fig. 3.19 is a photograph of the spark cathode by itself.

The nozzle assembly had to be modified for the laser test cell. The same nozzles were used but in different configurations. Various configurations and assemblies were tested to achieve maximum cooling. One such configuration is shown in Fig. 3.20. The nozzles are pitched at a slight angle ($\sim 7^{o}$) to cool more efficiently near the support rib in the center of the foil. The water intake is the copper tube in the middle and the air intakes are the two brass elbows. The aerosol injection system was essentially the same as that used for the simulation test cell.

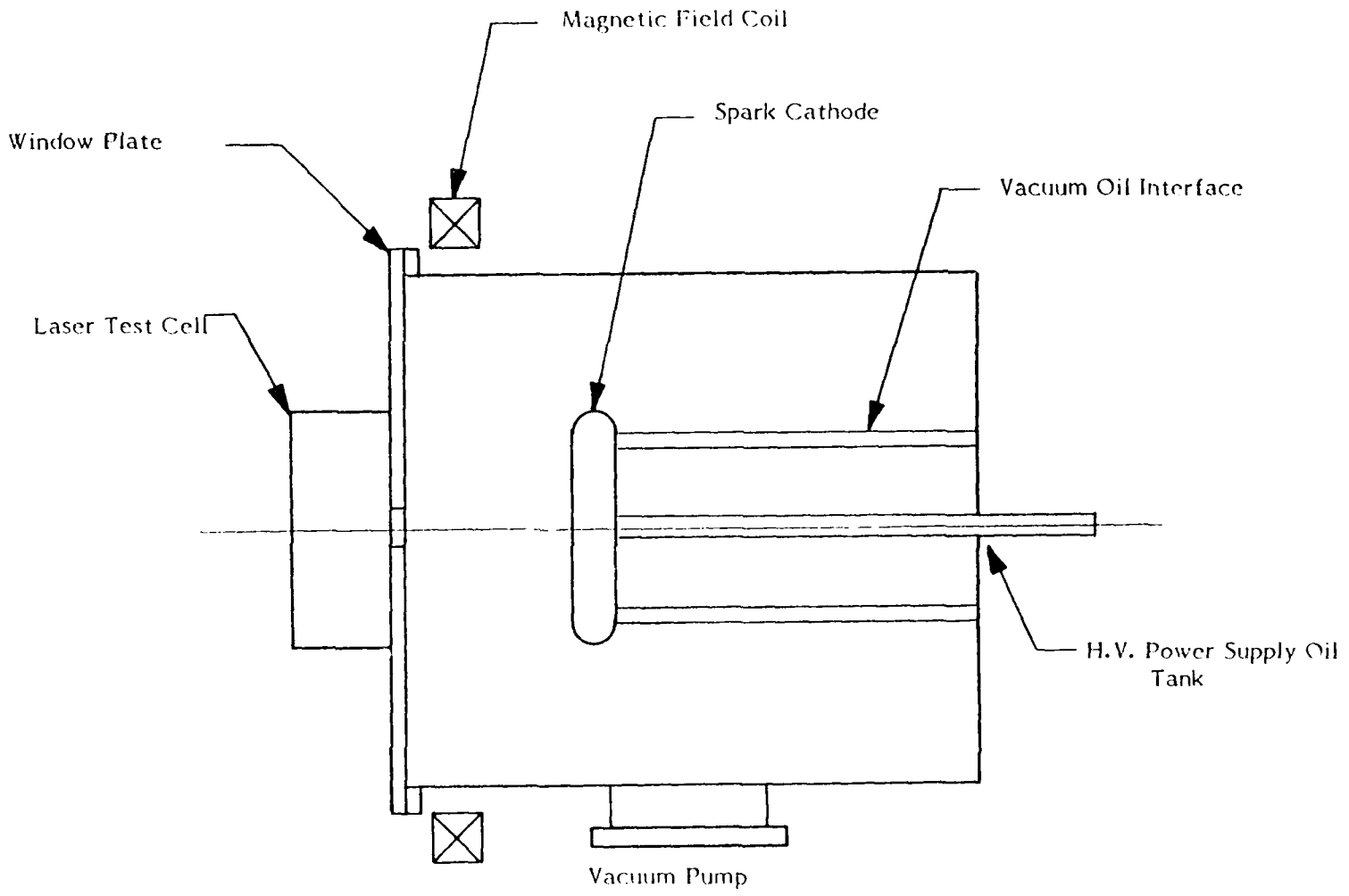

Fig. 3.15 Test Unit Schematic

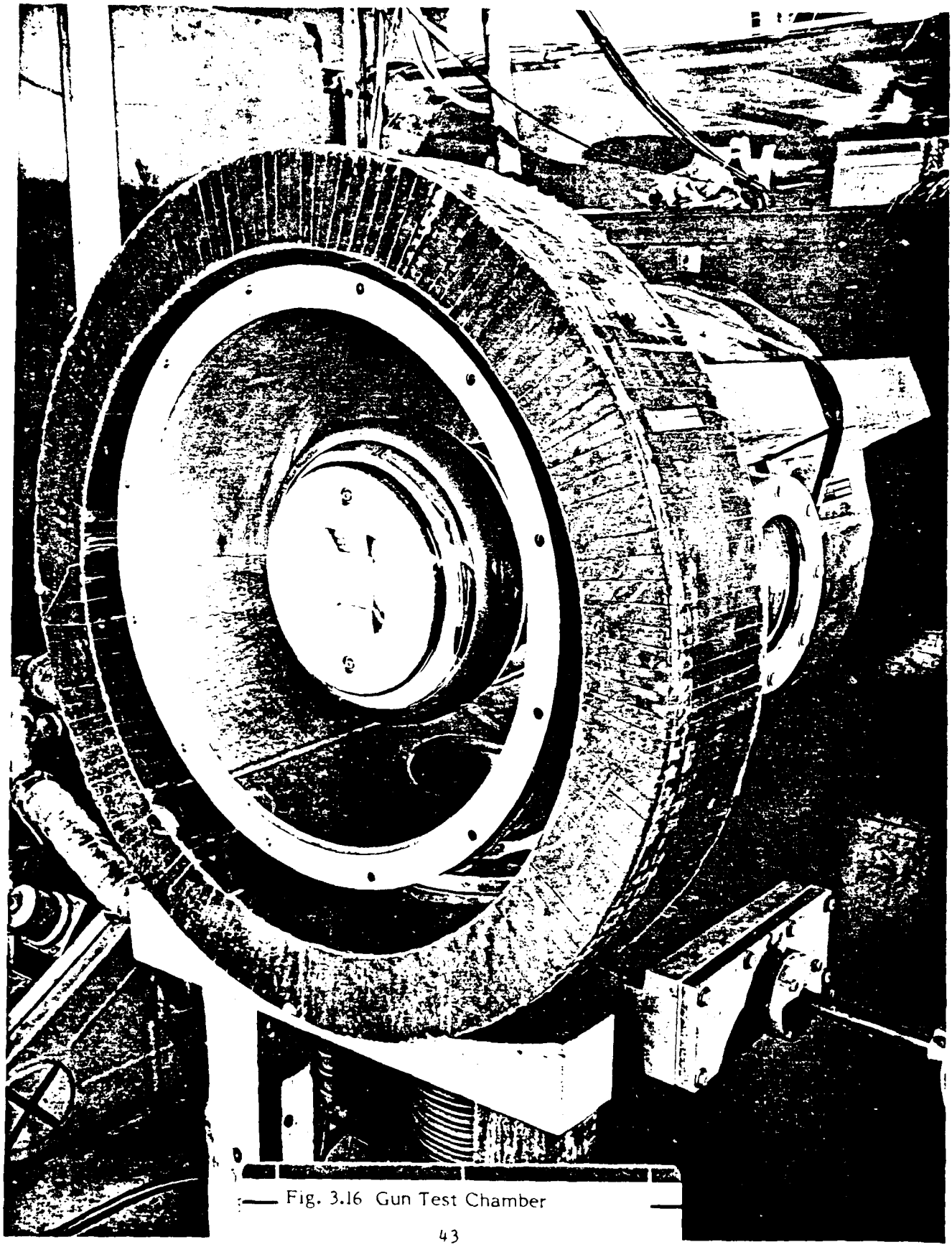

Fig. 3.16 Gun Test Chamber

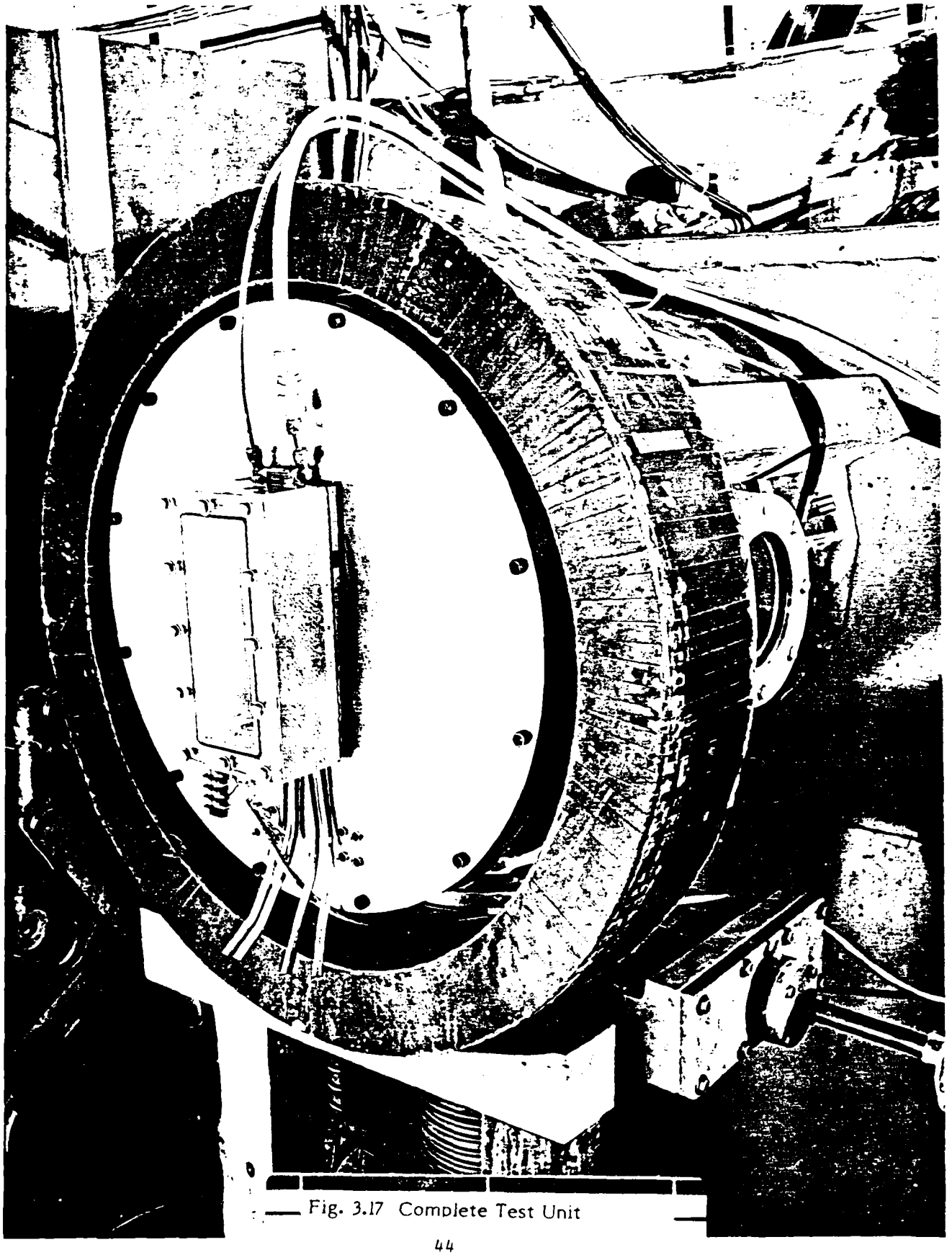

Fig. 3.17 Complete Test Unit

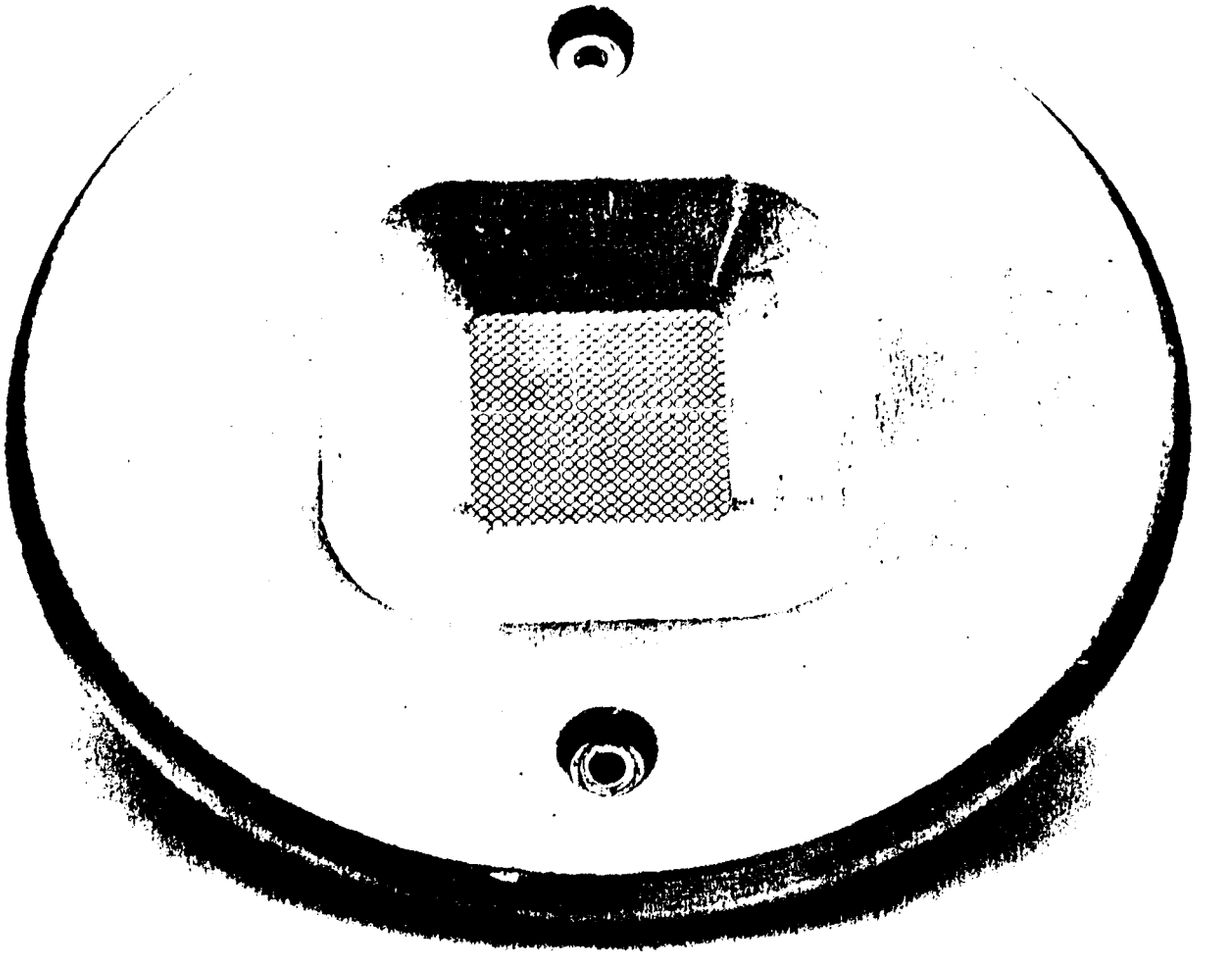

Fig. 3.18 Cathode Holder

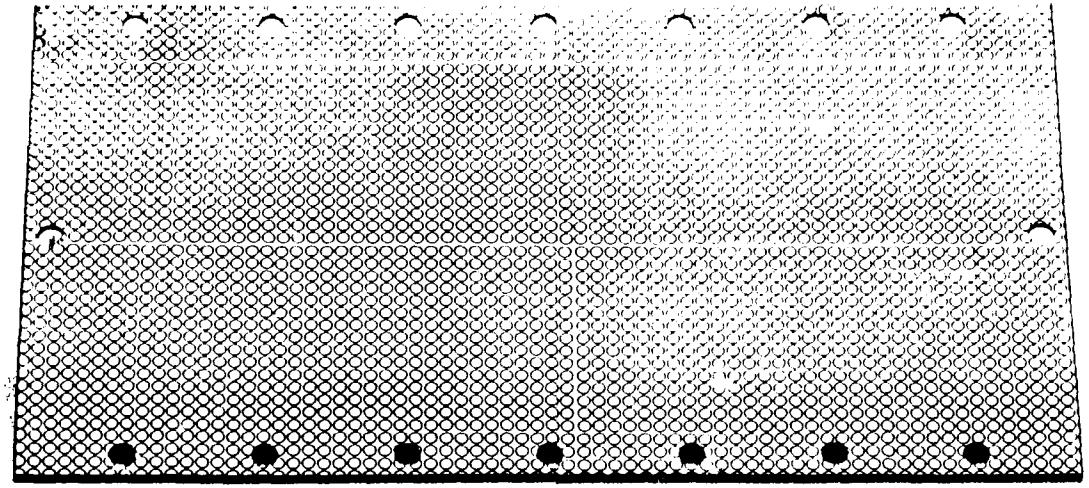

Fig. 3.19 Spark Cathode, 16 sites cm^2

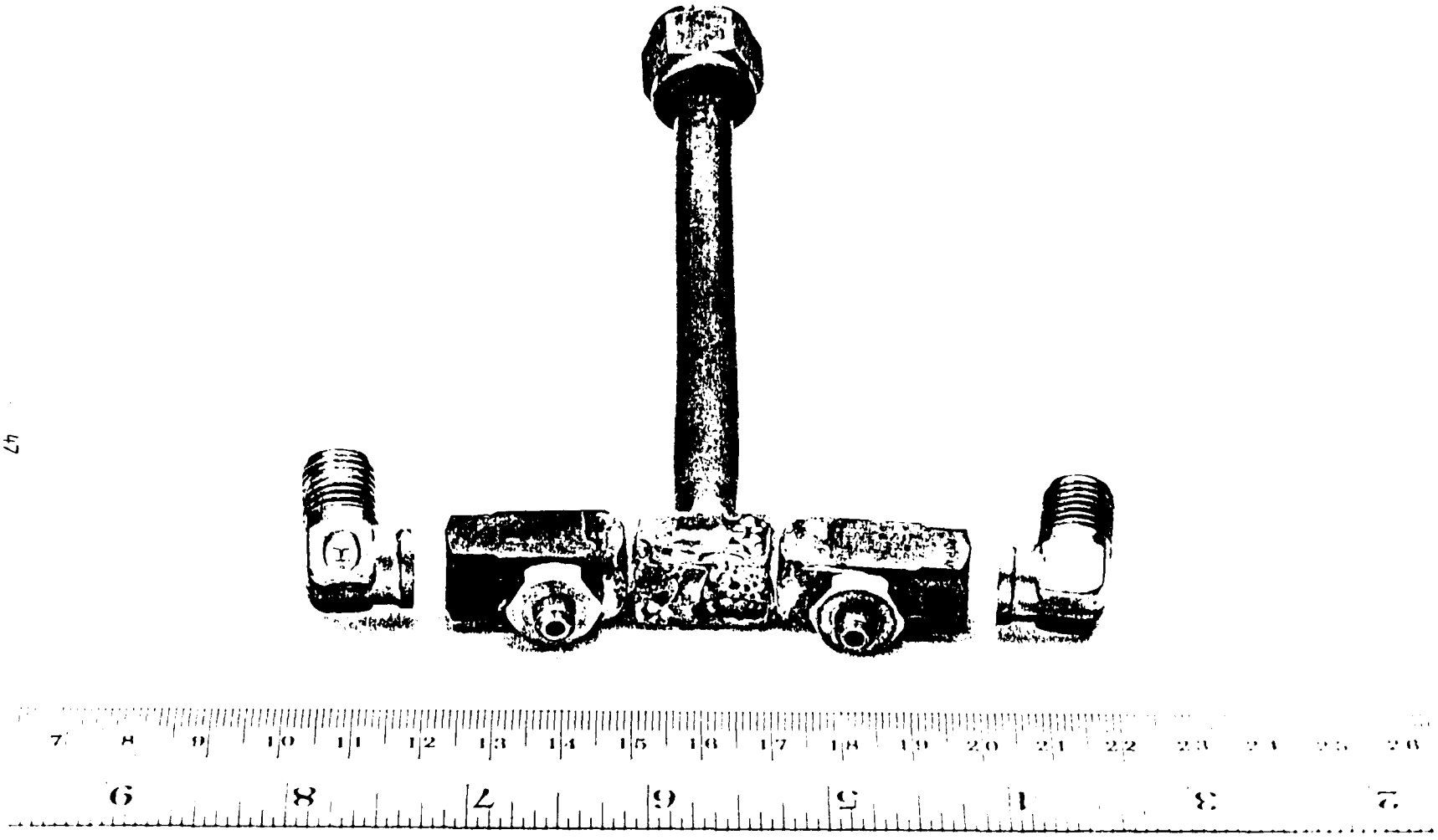

Fig. 3.20 Laser Test Cell Nozzle Assembly

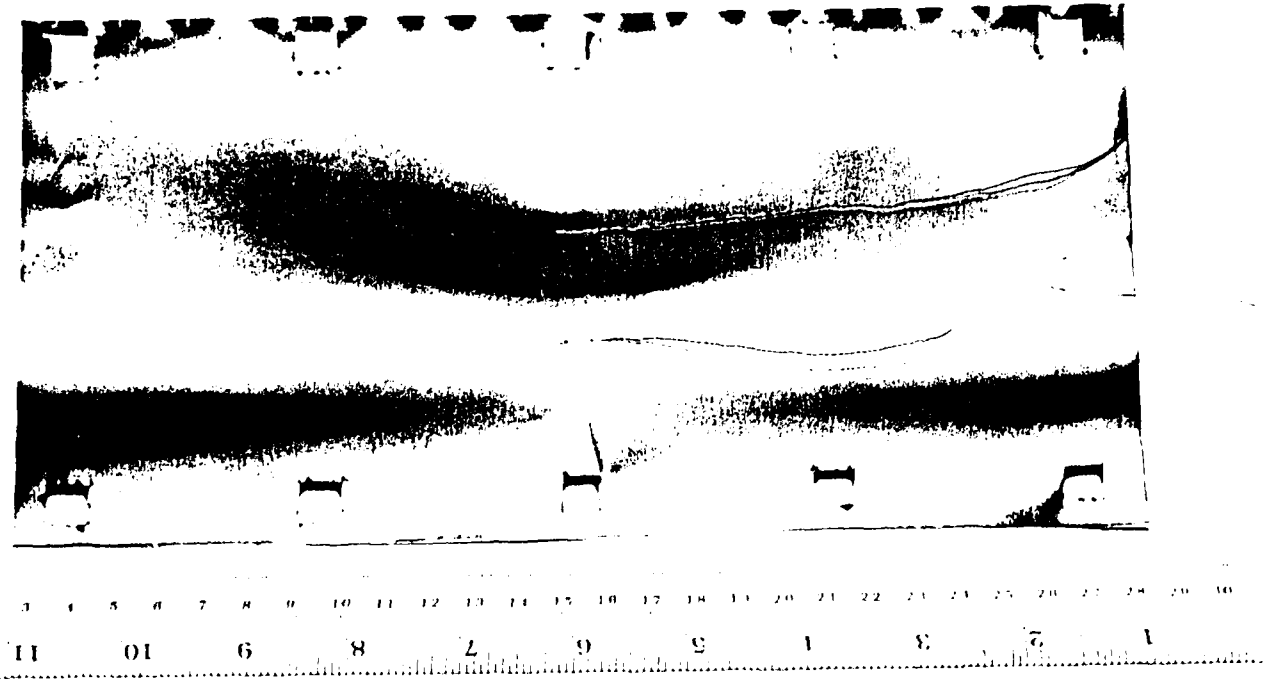

Fig. 3.21 Window Foil with Thermocouples Attached

5 mil thermocouple wire

Horizontal .5 sec/div.

Vertical 65°C/div.

80 cm/sec. gas flow

1 pulse

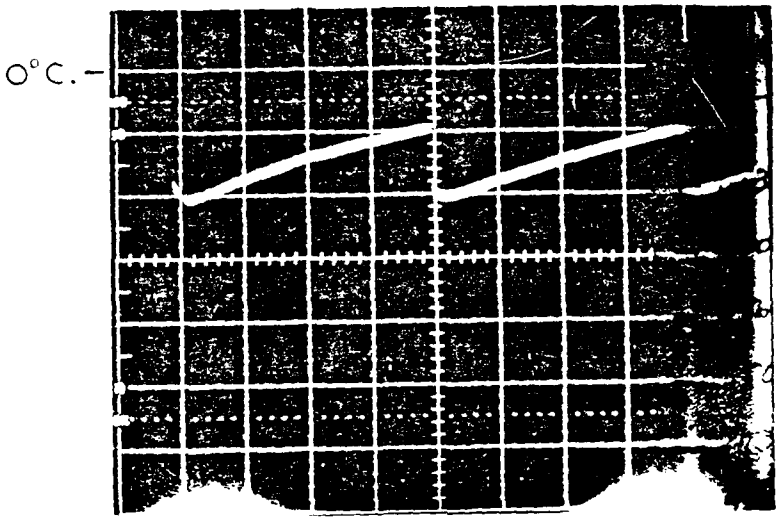

3 mil thermocouple wire

Horizontal .5 sec/div.

Vertical 65°C/div.

80 cm/sec. gas flow

1 pulse

Fig. 3.22 Response Times of Five Mil and Three Mil Thermocouples

Diagnostic requirements and diagnostic access were again an important factor in the test cell design as they were in the simulation test cell. The same diagnostic devices, flow meters and pressure gauges, that were used for determining the aerosol characteristics for the simulated foil test cells were used for the laser test cell. The input power to the e-beam gun was measured by monitoring the voltage and current output of the PFN. This was accomplished with resistive and capacitive voltage dividers and current transformers. The foil temperature distribution and the energy deposited in the foil were measured using 3 mil chromel-constantan thermocouples. The thermocouple wires were spot welded at the junction to the window foil in the path of the e-beam where the energy was deposited. The lateral heat transfer in the foil was again minimal compared to the heat transfer to the aerosol. Fig. 3.21 is a photograph of a one-half mil titanium window foil with two thermocouples attached to it. The thermocouple temperature measurements served two purposes: one was to calibrate the system, and the other was to measure the foil temperature under the actual phase transition cooling conditions. To calibrate the system, shots were fired into the foil with no aerosol cooling of the foil. In this mode the foil was acting as a calorimeter. The beam deposited a certain amount of energy in the foil per pulse, which would cause the temperature of the foil to increase. By measuring the temperature increase with the thermocouples, and knowing the specific heat and mass of the foil, the deposited energy per pulse could be determined. This was done for specific voltage and current settings.

Another feature that was incorporated into the temperature measuring system was an instability interlock. A thermocouple attached to the foil inputed an interlock to the trigger generator, which was set at a specific voltage, above which the foil would be in danger of rupturing. Thus, the interlock system would shut down the gun if an instability occurred and the foil temperature went above- $\sim 100^{o}C$, which was the normal operating temperature.

This section has described the experimental apparatus and techniques which were used in both phases of the program. The components which made up each of the two test cells were described. Also the technique used in testing were defined and explained.

SECTION 4

EXPERIMENTAL RESULTS

In order to demonstrate the applicability of phase transition cooling, two separate experiments were planned. In the first experiment, a full 50 cm wide mockup of the laser window was used as was described in the previous section. The heat input to this system was by means of resistive heaters so that the duty factor was 100% without the characteristic transient power histories described in Section 2. The second experiment used a pulsed electron beam to thermally load the foil in the time varying manner discussed. With the electron beam, energy was deposited in the foil in approximately 2 microseconds with a separation between pulses of 10 milliseconds.

4.1 Simulated Foil Tests 100°C

The first task of the experimental program was to determine if the phase transition cooling accomplished in the IR & D task could be scaled in area and to a geometry more consistent with a foil window. The IR & D task looked at areas less than 1 square centimeter. The first task was to investigate the cooling characteristics for a foil type geometry. The area to be cooled measured 5 x 25 square centimeters. The aerosol was injected along the 25 centimeter dimension and was run in an open channel configuration so that the pressure in the channel was approximately atmospheric. Heat was supplied in only one side of the system by way of the copper blocks discussed in Section 3 with the opposing side separated from the atmosphere with either a Kapton foil or glass. The results of these tests are shown in Fig. 4.1. The surface temperatures indicated were monitored with thermocouples resistance welded to the simulated foil surface. The general characteristics are of course quite similar to those shown previously in Fig. 2.2. The efficiency with which the aerosol was utilized in shown in Fig. 4.2. The efficiency number is arrived at by experimentally determining the maximum power that can be suplied to the heaters for a given flow rate

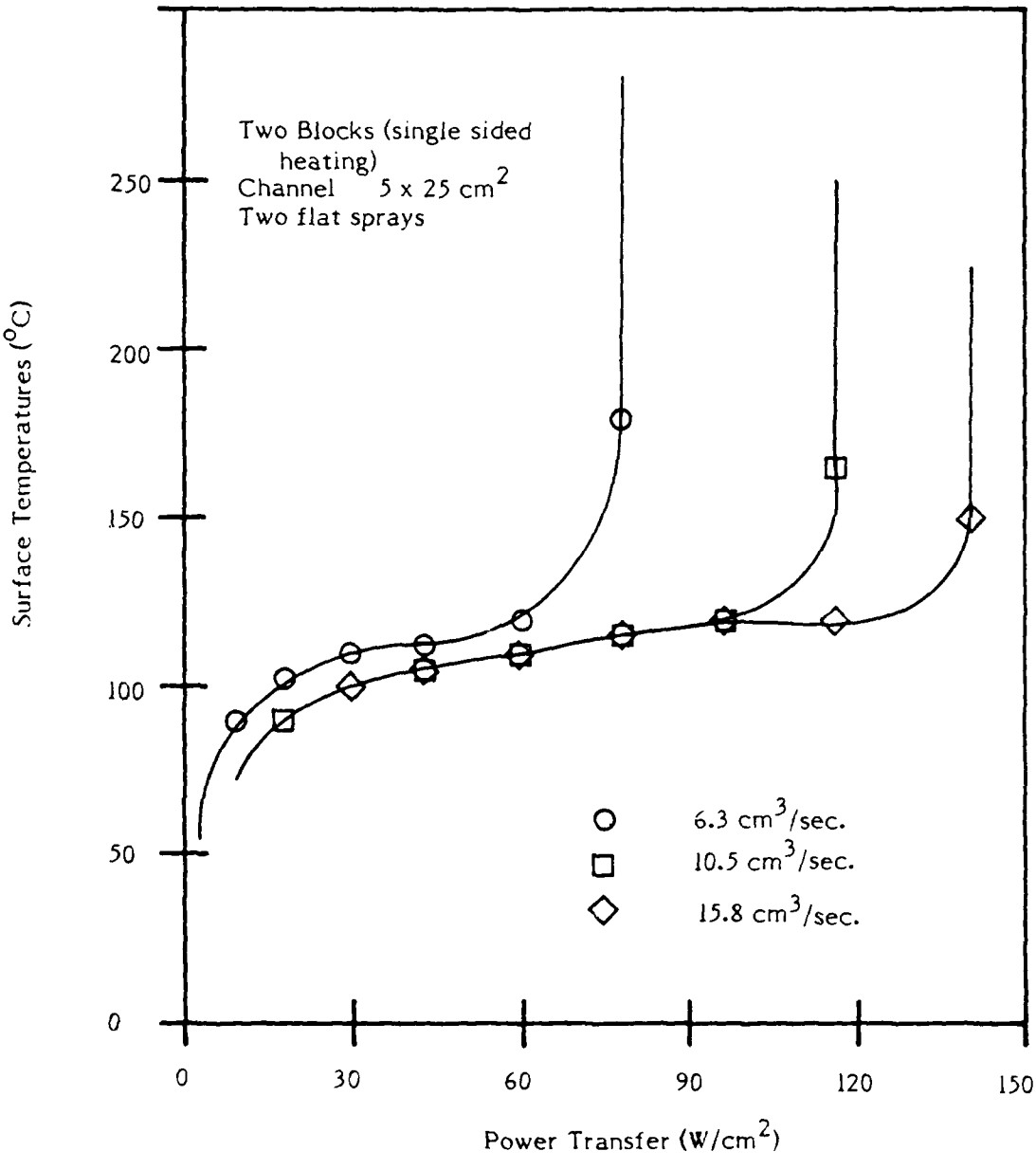

Fig. 4.1 Power Transfer Characteristics

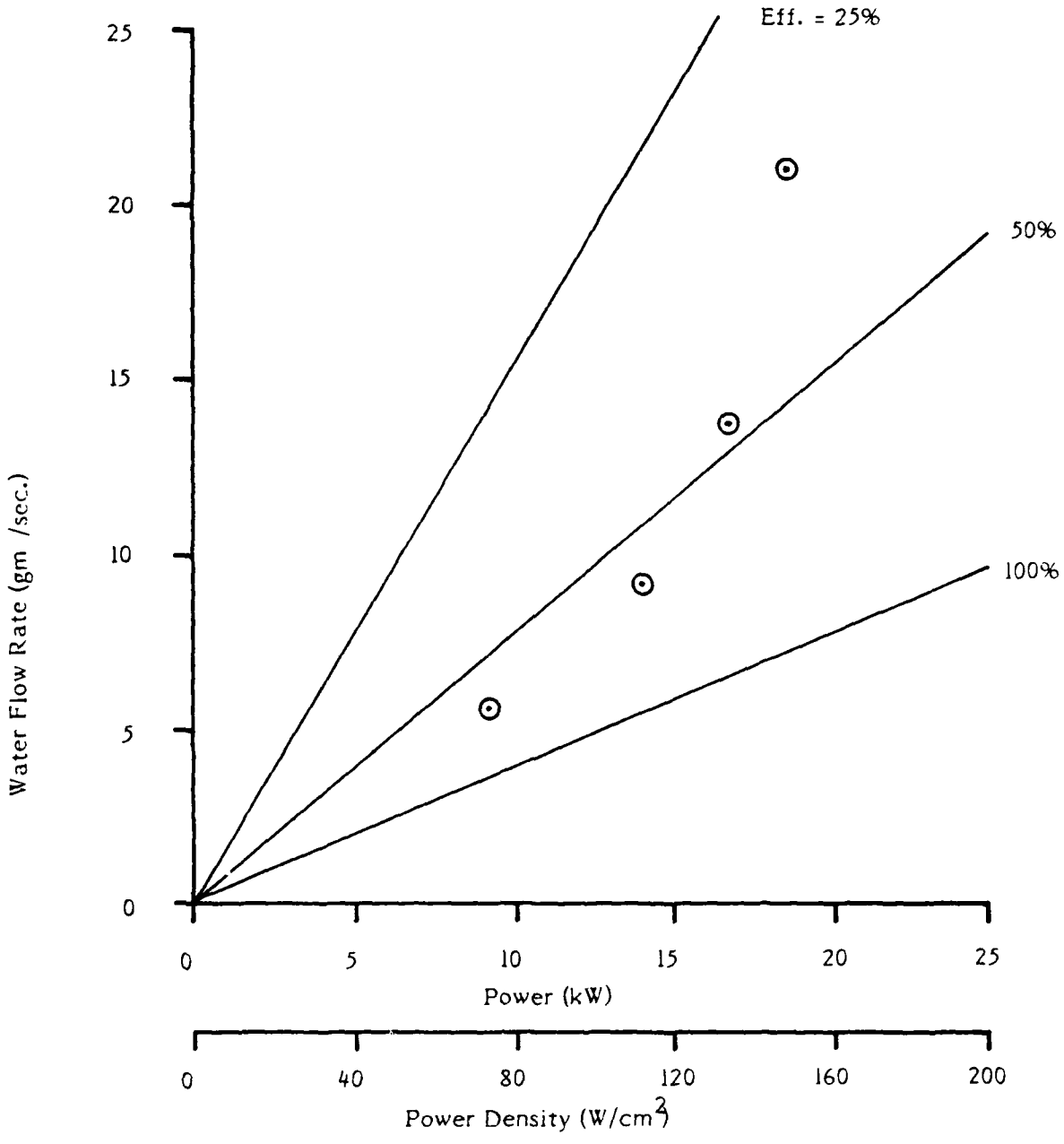

Fig. 4.2 Water Utilization Efficiency

Two blocks; 5 cm x 25 cm channel ; single sided heating
Two nozzles - flat spray; 684 cm/sec. air

of water without thermal runaway occuring whereby the substrate temperature significantly exceeds the boiling point of the liquid. If 100% efficiency was obtained, this would mean that for each gram of water supplied to the system 539 calories could be dissipated, if the initial temperature of the water was 100°C. An efficiency of 50% implies that only half of the water injected to the system was converted to steam and that the remaining 50% exited from the system still in the form of liquid water. For the above two figures two nozzles were used and both were the flat sprayed configuration. The water quantity listed corresponds to the sum of water supplied to both nozzles as does the amount of air listed.

After these preliminary tests the full length geometry was assembled and similar tests were run. The area corresponded to 5 x 50 square centimeters with the heat again being inputed only to one side, with the flow in the 50 cm dimension. The distance between the simulated foil and the glass or Kapton was one centimeter. This corresponds to an aspect ratio of 50:1. The procedure was very similar to that described previously. Thermocouples were attached along the entire length of the flow channel. Temperature readings were taken when the complete system was stabilized. The results of some of these measurements are shown in Fig. 4.3. Three different power loadings are shown in this figure ranging from 68 watts square centimeter to 103 watts per square centimeter. The unique property of the phase transition cooling is readily apparent in this figure. For a constant water and gas flow rate power was changed by more than 50% with an only insignificant change in the temperature of the substrate. The temperature change that did occur was the order of a few percent and can very well be the result of a thin film buildup of the substrate. Power transfer rates encountered throughout these experiments are very large compared to most industrial standards. To illustrate this, Table 4.1 indicates the ΔT that would be experienced across a 1 mm thick sample at a power loading of 100 W per sq. cm. for various materials.

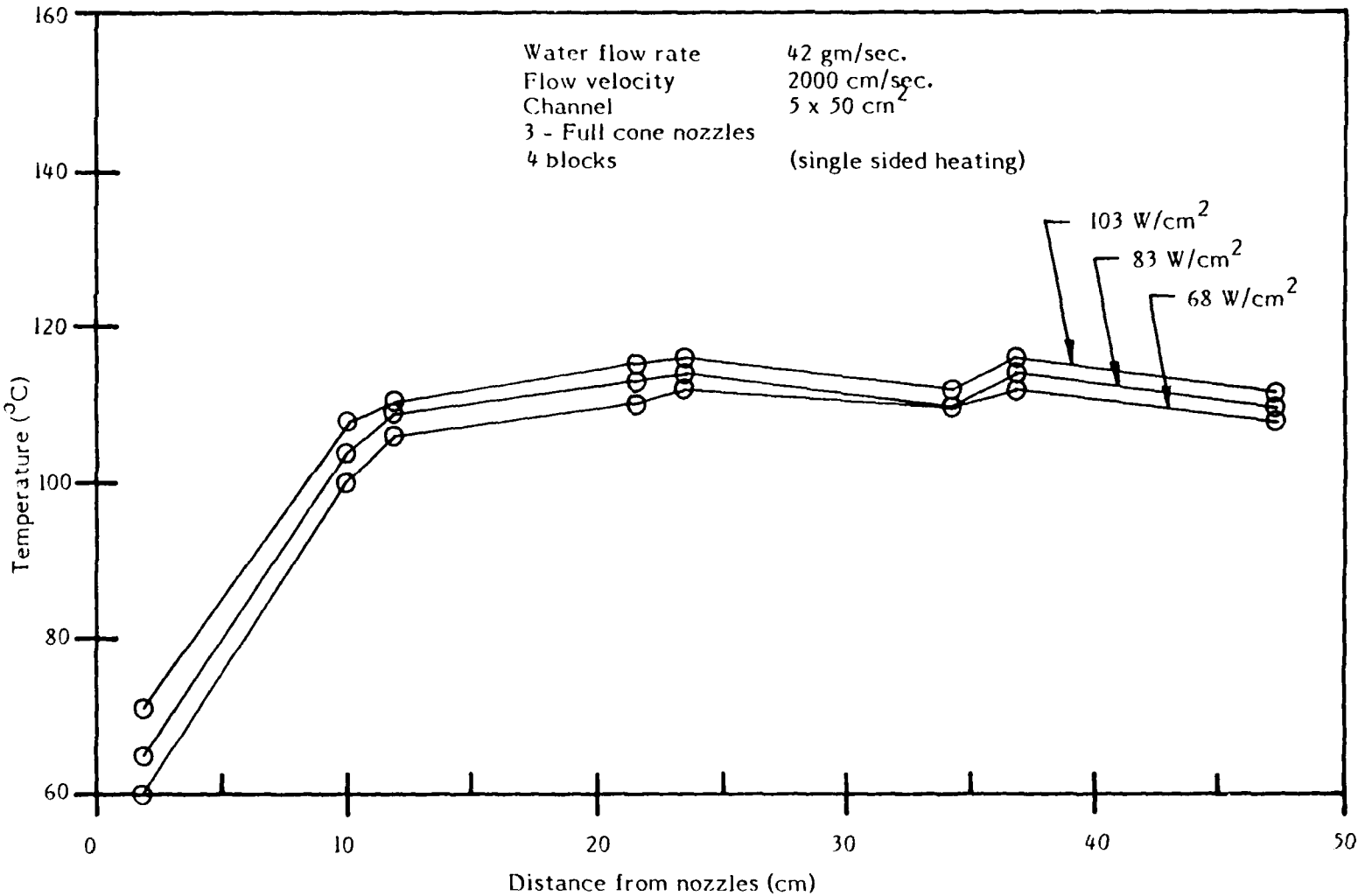

Fig. 4.3 Independence of Temperature on Power Loading

TABLE 4.1

Temperature Differential Across Various Materials

	t	ΔT
Steel	1 mm	22°C
Copper	1 mm	2.6°C
Stainless Steel	1 mm	75°C
Water	0.1 mm	150°C
Limestone (~ scale buildup)	0.001 mm	61°C

ΔT for 100 W/cm^2 - power transfer

A similar set of data was taken for the same 5 x 50 sq. cm. apparatus however, this time only a single nozzle was used with consequently lower power density loadings. This data is shown in Fig. 4.4. What is apparent from both the previous data is that for the situation where there is a constant heat flux into the foil the temperature will be at the boiling point with very small deviations. It also implies that temperature measurements are of limited value from an experimental point of view as long as stable operation is achieved. The efficiency for each of these two previous experiments is shown in Fig. 4.5.

Gas cooling was briefly investigated with the same apparatus as a means to determine if any of the cooling observed earlier is a result of the gas flow. The power input to the system in the gas flow rate were adjusted so that the foil temperature was at the 100°C level. The results of these tests are shown in Fig. 4.6. The amount of heat extracted by the gas flow in terms of the previously reported numbers is insignificant. The effect of gas flow, except as it relates to transport of the water, can be ignored.

In order to more closely simulate the laser geometry a second set of heated blocks were added on top of the first set. Heat input was then provided to both sides of the channel. Tests were done with both a 5 x 12.5 cm^2 and a 5 x 50 cm^2 geometry. The results of these tests are shown in Figs. 4.7 and 4.8 respectively. In both figures the power density of watts per sq. cm. corresponds to the total power input to the system, divided by the total surface area impacted by the flow. For the 5 x 50 sq. cm flow channel the total surface area is 500 sq. cm. that is both sides are summed separately. The nozzles used limited the total amount of water that could be supplied for the 50 cm case, and we could not investigate the higher power density loadings.

It was observed that when stable operation was achieved a very thin film of water would be present on the foils. As unstable operation was encountered, that is as the total power was increased beyond the capabilities indicated in the figures, a "drying out" of the surface would occur. This drying out would occur from the exit end of the system and progress towards the nozzle as the power was correspondingly increased. We relate this problem to the inability of the aerosol stream to come in contact

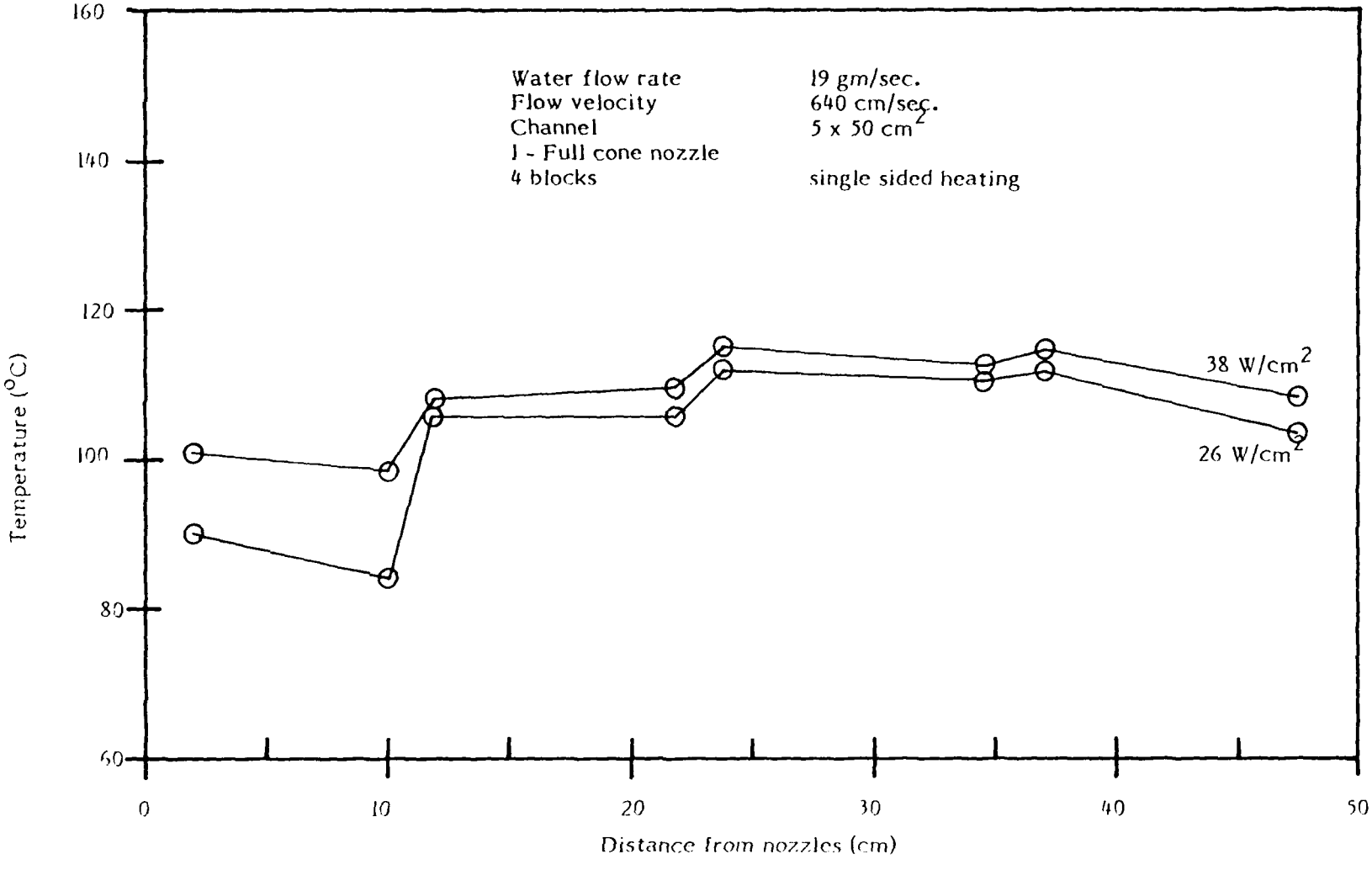

Fig. 4.4 Temperature Distribution

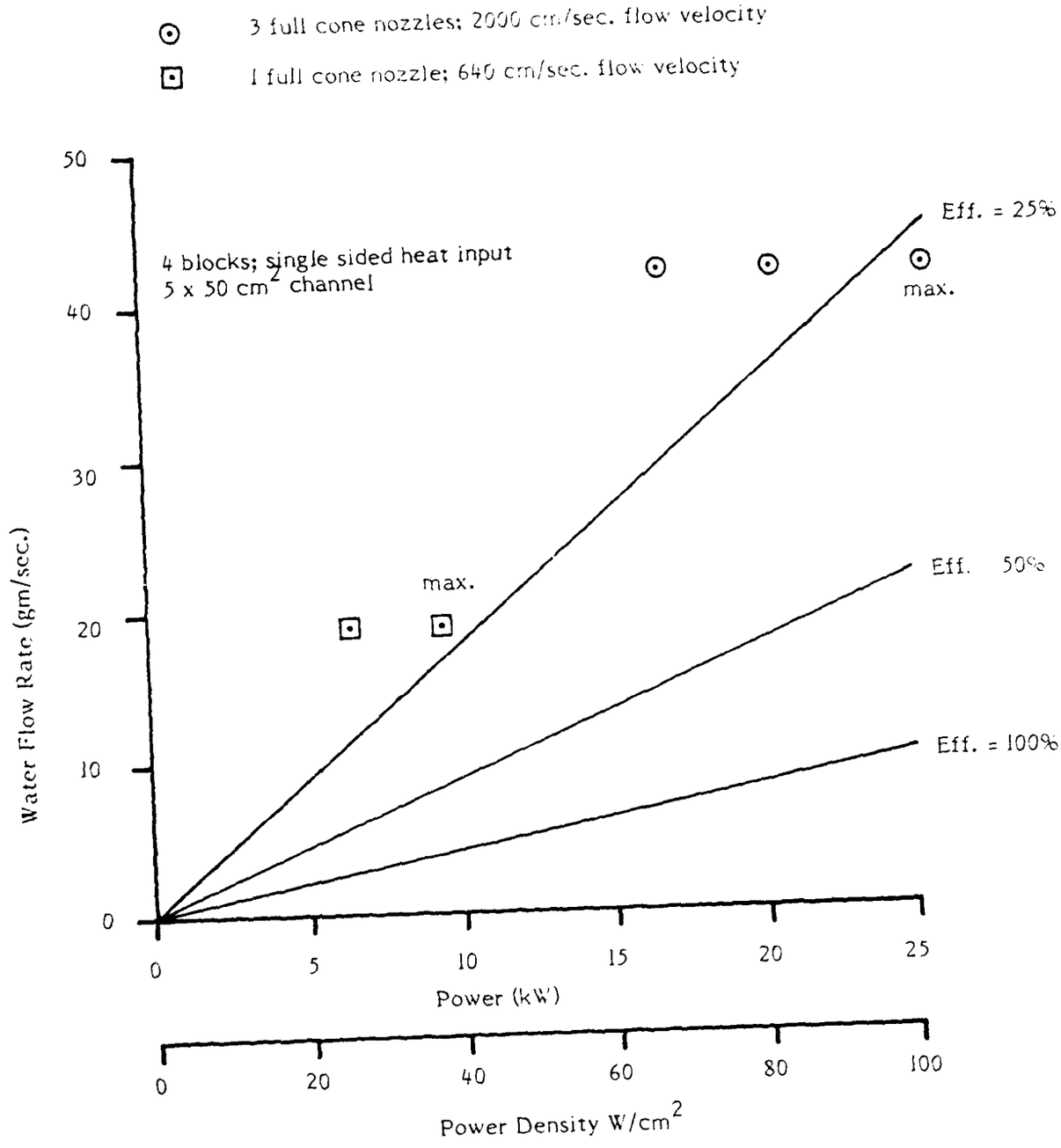

Fig. 4.5 Water Utilization Efficiency

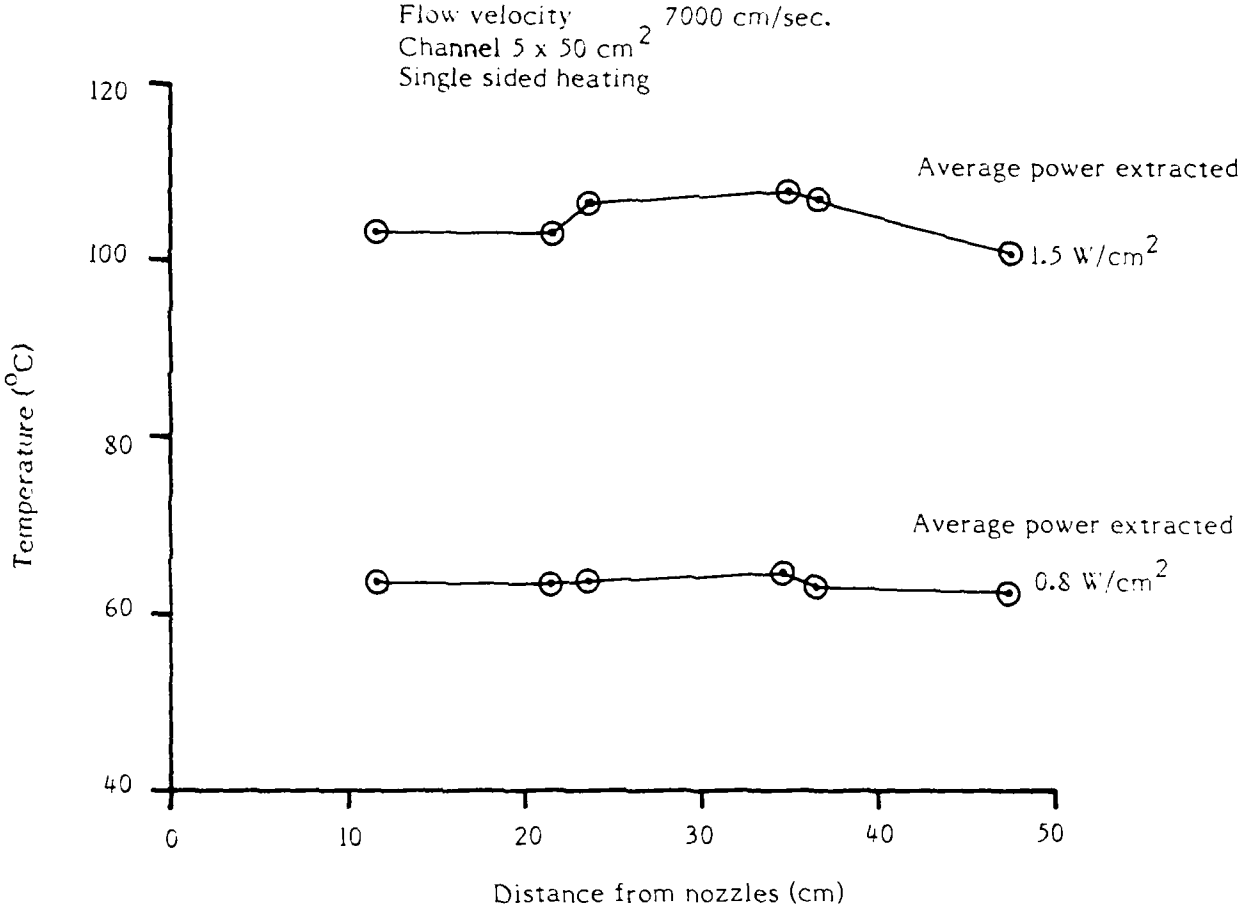

Fig. 4.6 Gas Cooling

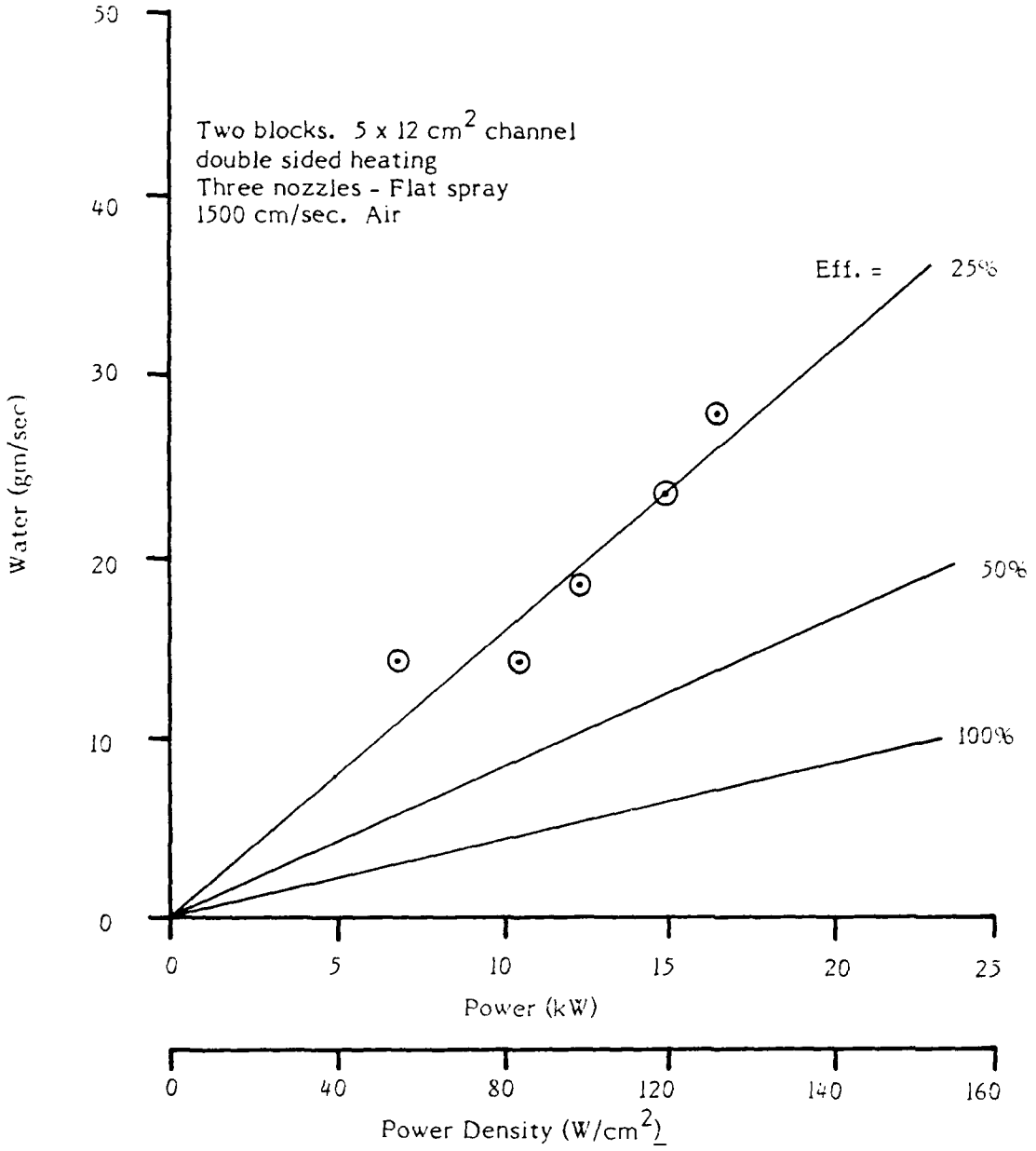

Fig. 4.7 Water Utilization Efficiency

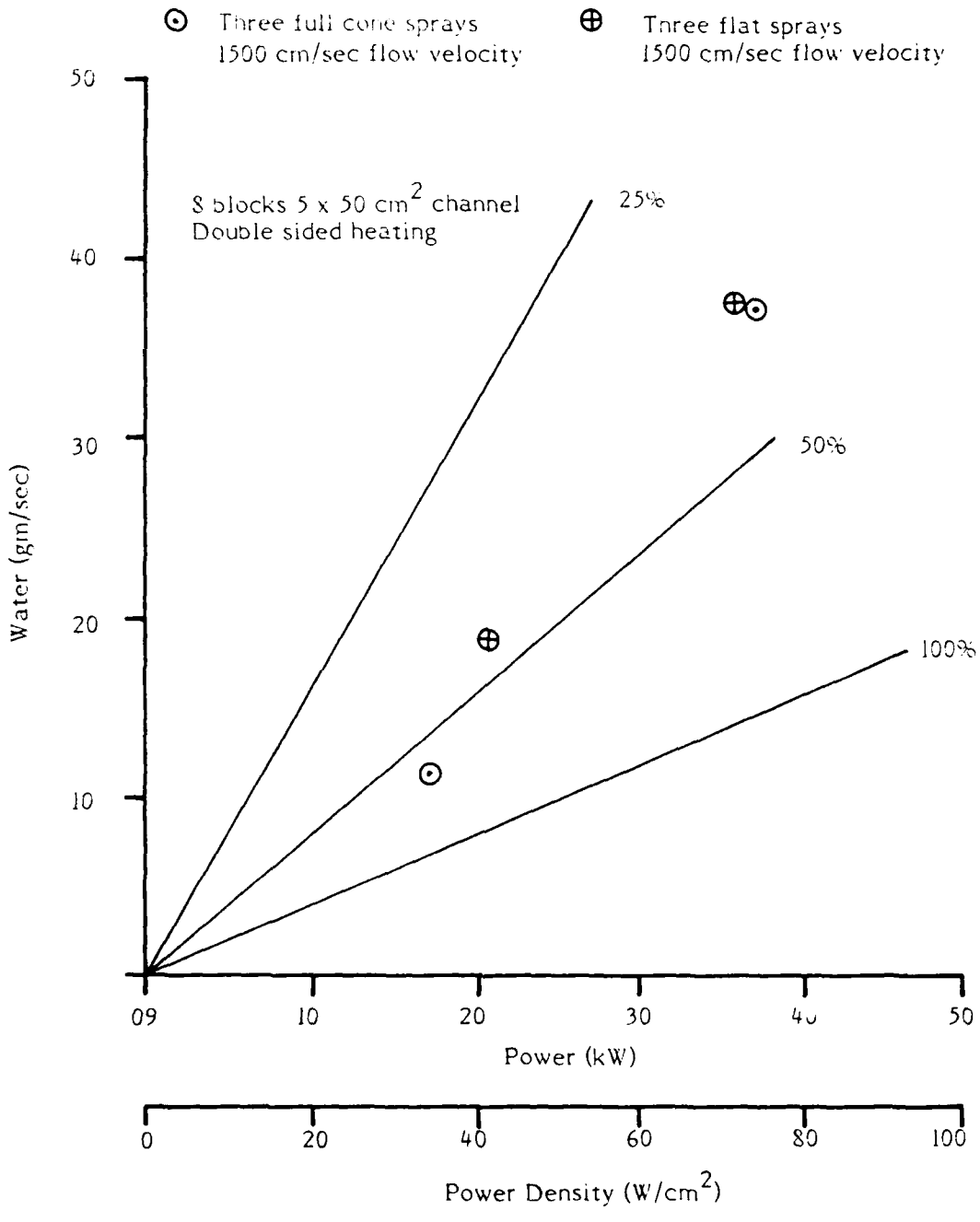

Fig. 4.8 Maximum Power Transfer of Water

with the surface. The water droplets become confined, for the high aspect ratio systems, to the center of the channel with the flow not having sufficient turbulence to bring these droplets into contact with the foils. A test was undertaken in an attempt to generate additional turbulence in the system. Using the same 5 x 50 cm^2 system, however with heat input to only one side, a turbulence inducing flow plate was inserted into the system approximately 25 cm from the input end. For the given conditions an increase of power transfer capability from 26 to 67 watts per sq. cm was observed before unstable operation occured. Similar increases in power density did not occur for correspondingly higher flow rates. This was not sufficiently explored and may have been the result of experimental difficulties with the system. Two temperature distributions, are plotted in Fig. 4.9; one with the flow plate and one without the flow plates. At a position downstream of the nozzle plate a small but significant temperature decrease can be observed indicated the flow was again forced to contact the side walls.

Aerosol distribution in the flow channel was investigated by means of a laser scattering experiment described previously. Data from the measurement of light scattering by the aerosol with and without heat input are shown in Fig. 4.12. Several measurements (between five and ten) were taken at each distance from the nozzles. The raw data were reduced by calculating the mean value and the standard deviation at each location; the vertical error bar in Fig. 4.12 represent the standard deviation.

A qualitative explanation for the observed results is offered as follows. Relatively large scattering is observed close to the injection nozzles because all of the injected droplets exist (none have evaporated) and are concentrated near the axis because the aerosol flow is still expanding. In the case without heat addition, the aerosol droplets hit the walls of the channel and coalesce into a film of water which clings to the walls and is blown out of the end of the channel. The removal of aerosol droplets from the volume is therefore approximately linear with distance in the data shown.

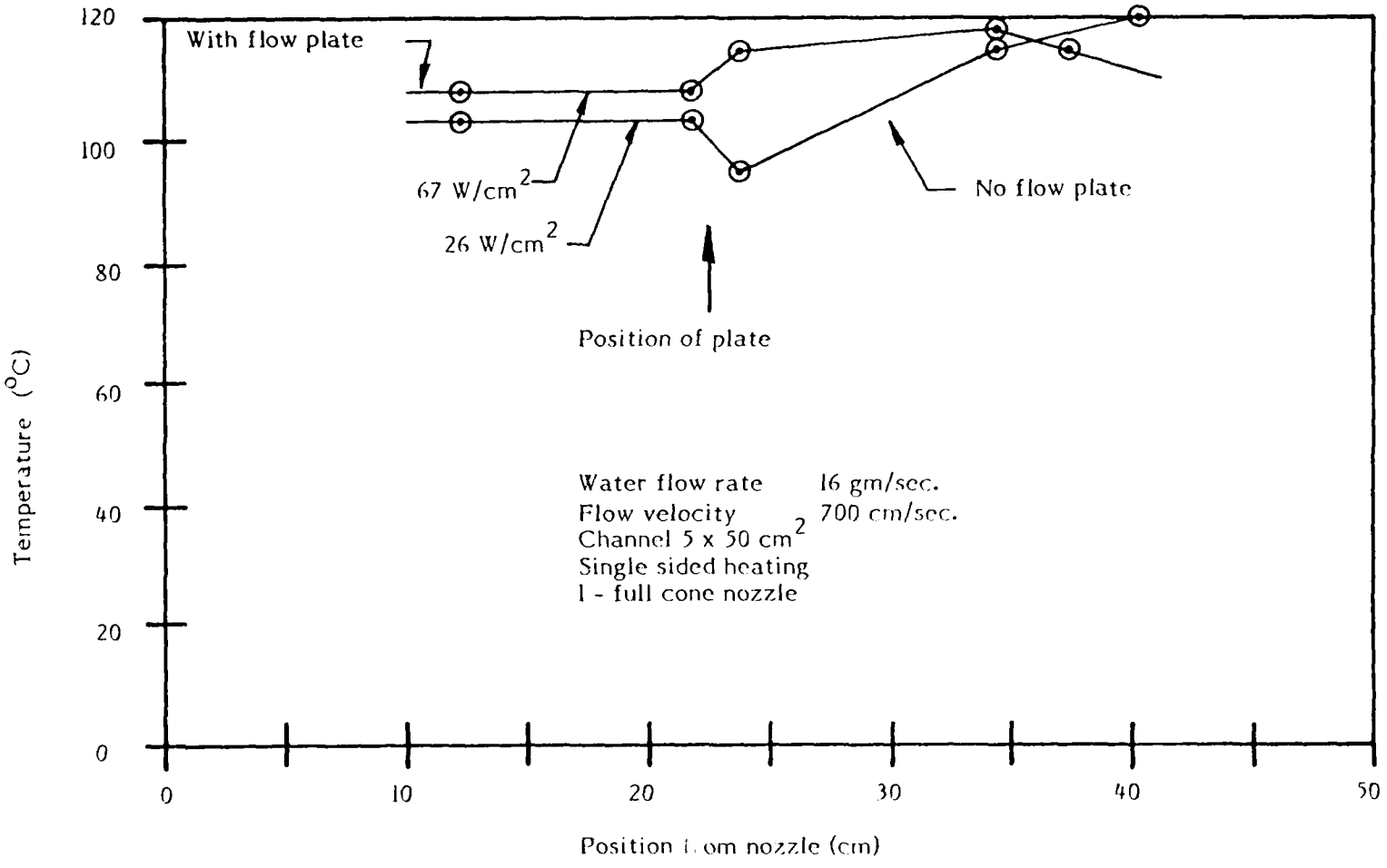

Fig. 4.9 Temperature Distribution - Turbulence Plate

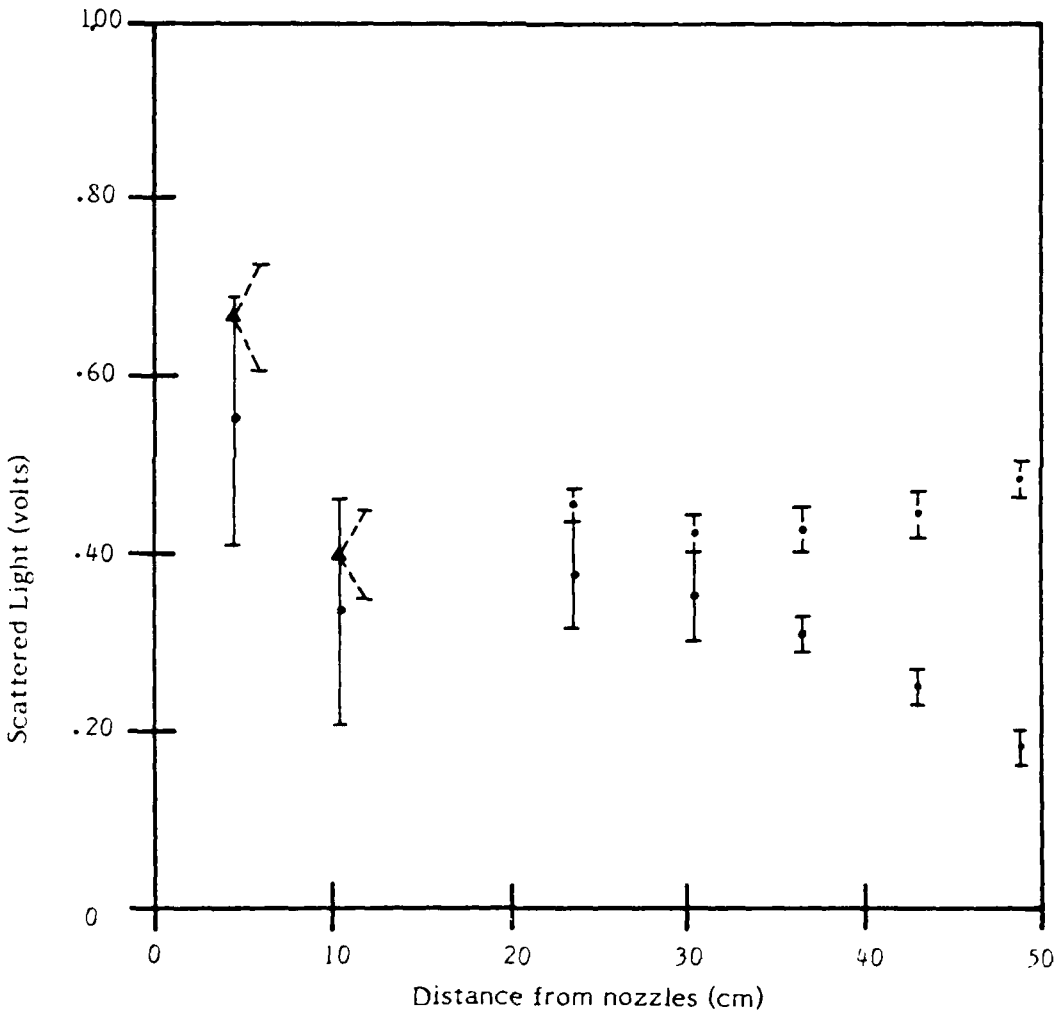

Fig. 4.12 Light Scattering from Aerosol vs. Distance from Nozzles

When heat is added, the rapid evaporation of the aerosol droplets as they strike the channel walls, and the expansion of the water vapor, changes the flow pattern in the channel and tends to concentrate the aerosol in the center of the volume for longer distances, creating a slight increase in the signal strength.

4.2 Simulated Foil Tests - 200°C

A similar set of experiments to those described earlier was performed using ethylene glycol as the liquid. Ethylene glycol was utilized so that cooling could be demonstrated with the foils at a 200°C average temperature, corresponding to a possible operating condition for the laser system. The temperature at which stable operation was achieved as shown in Fig. 4.10 was clearly at the 200°C temperature as anticipated. For these tests the flow channel was 5 x 37 cm^2. The amount of power transferred at a given flow rate of the glycol was of course less than water by of differences in heats of vaporization. The efficiency of utilization shown in Fig. 4.11 is of the same order as that previously demonstrated where water was the liquid.

4.3 Electron Beam Tests

The pulse modulator for the electron beam had a limited power capability that was inadequate for the testing of a full 5 x 50 cm^2 device. Full power testing was performed with a smaller device using a 7 x 7 cm^2 beam. The beam was laterally constrained with an axial magnetic field and was uniform over this area. Full diagnostics were installed in the modulator and the electron gun, however, the principle diagnostic were the foils themselves.

Attaching a thermocouple to the foil allowed the foil to act as its own calorimeter. We were able to exactly determine the power input to the foil, including all electron backscatter, by measuring the Δ T produced in the foil by one electron pulse. The foil power loading was varied not only by altering the electron beam but also by increasing the foil thickness so that more of the electron energy was deposited.

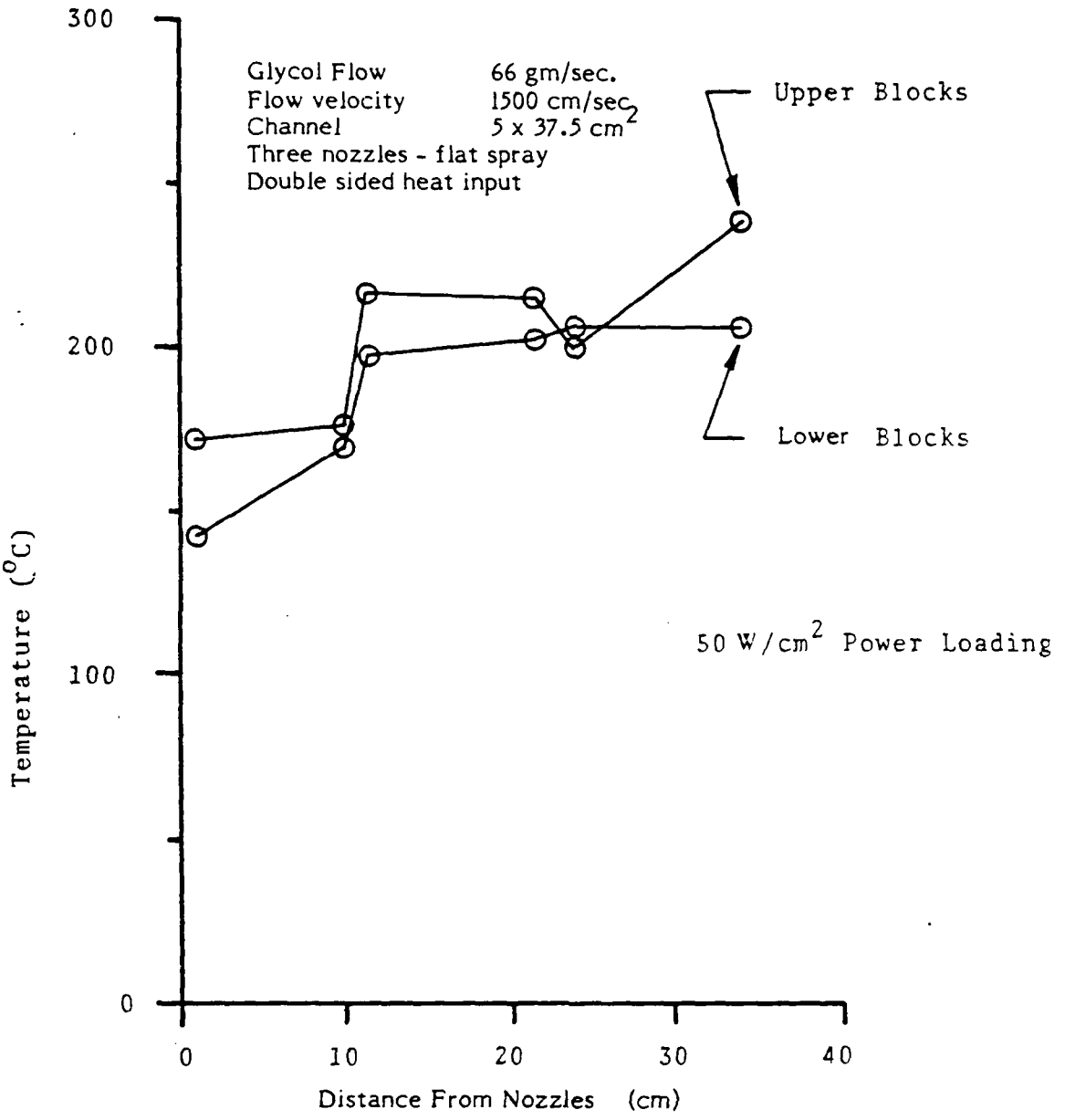

Fig. 4.10 Temperature Distribution - Ethylene Glycol Coolant

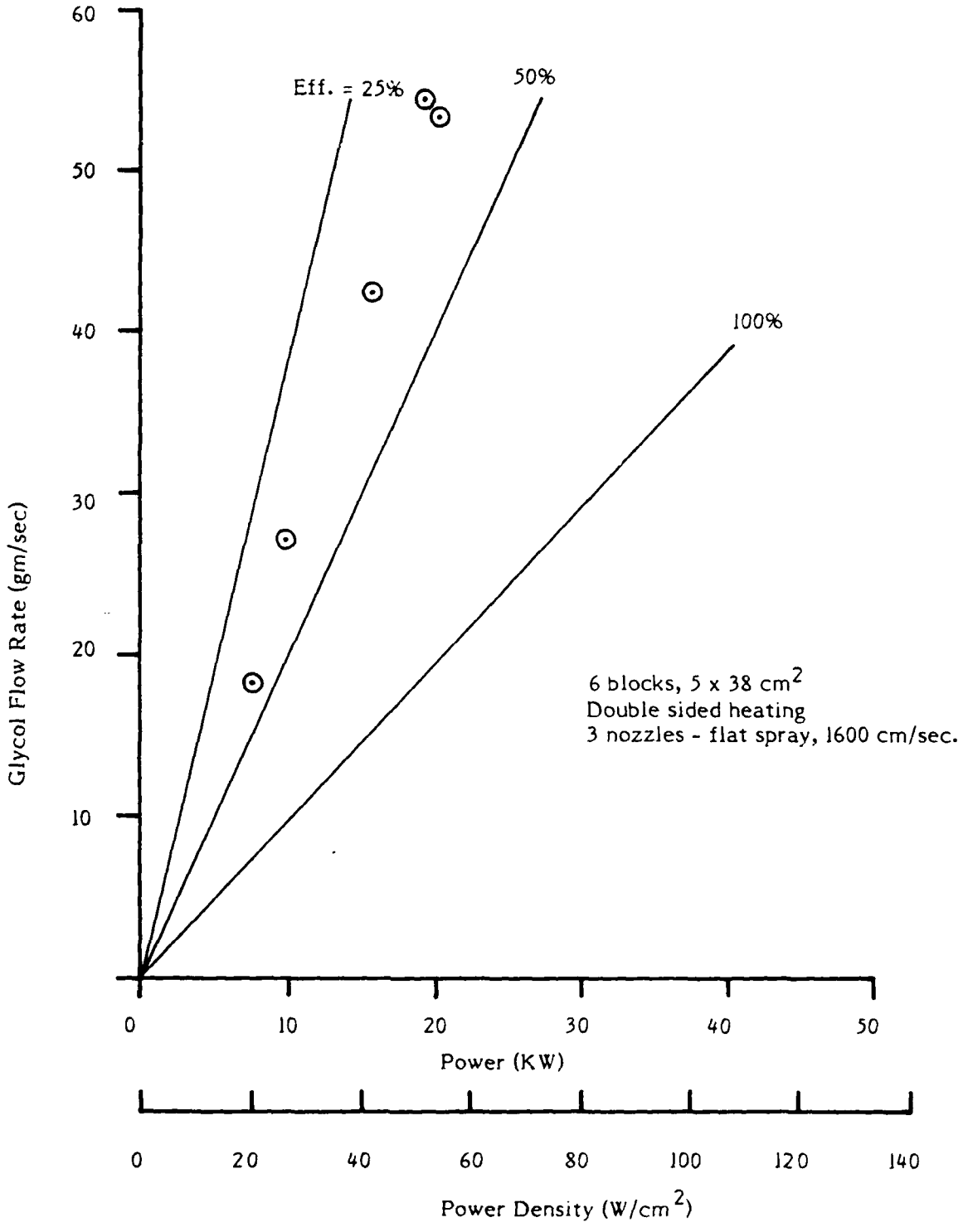

Fig. 4.11 Ethylene Glycol Utilization Efficiency

An example of this is shown in Fig. 4.13. The oscillogram shows the foil temperature as a function of time. The sweep rate is 10 msec/1 div and the vertical scale is approximately 65°C/div. Each of the three pulses raises the foil temperature by 65°C to a final temperature close to 200°C. Only a slow air stream was flowing in the channel so no significant cooling was taking place between pulses. For the 1 mil (0.0025 cm) stainless steel foil used this ΔT corresponded to a power loading in the foil of 70 W/cm^2. Similar measurements were performed before any cooling demonstration experiments were done.

When the water flow is added to the system, the corresponding oscillogram shown in Fig. 4.14 is generated. In this situation nine pulses were applied to the foil each separated in time by 10 msec, corresponding to the same 70 W/cm^2 power loading. The vertical sensitivity for the two oscillograms is the same. The characteristic phase transition behavior is again observed with the final, stable temperature very near 100°C. Although the thermocouple response time is marginal to observe the effect, the temperature waveform illustrates the characteristics of the two rate behavior postulated in Section 2 (see Fig. 2.5).

As we had done for the constant input power case previously described, gas cooling was also investigated. By applying several pulses in quick succession to the foil the foil temperature would reach 400°C. Differentiating the temperature waveform yields the cooling rate and hence the heat transfer for the system. This is illustrated in Fig. 4.15. For practical purposes the heat transfer as a result of gas flow is again insignificant.

Several different nozzles and nozzle flow geometries were investigated to determine maximum cooling rates. Efficiency of aerosol utilization was not stressed; the relatively low aspect ratio of 5.5 would make interpretation of the efficiency difficult in consideration of a full scale geometry.

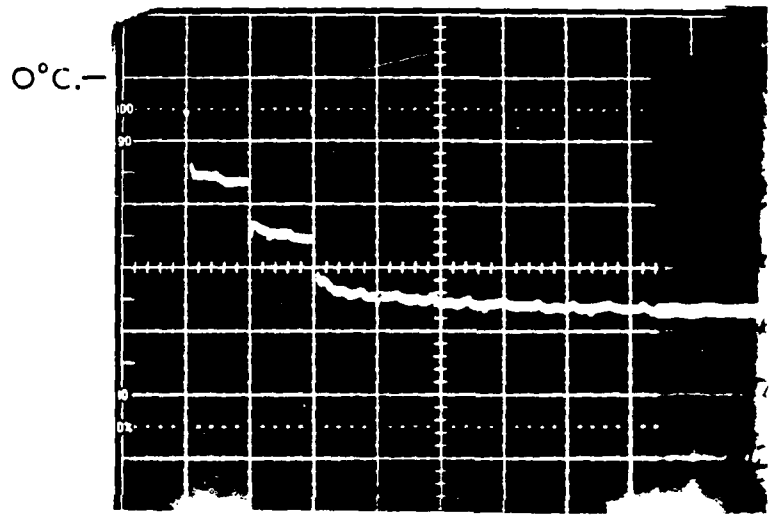

Horizontal 10 msec/div.

Vertical 65°C/div.

Three pulse

Fig. 4.13 Thermocouple Time History

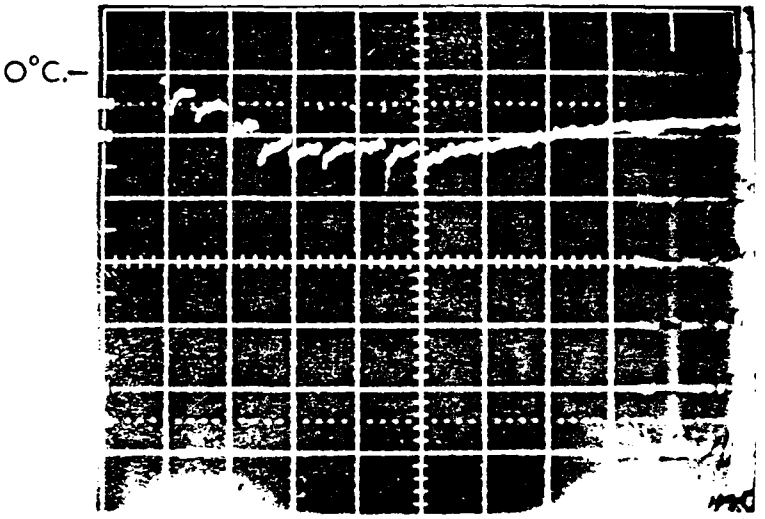

Horizontal 20 msec/div.

Vertical 65°C/div.

Nine pulse

Fig. 4.14 Thermocouple Time History - Phase Transition Cooled

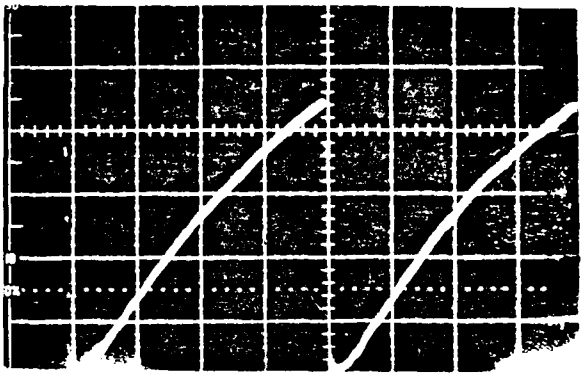

Horizontal .5 sec/div.
Vertical 65°C/div.
80 cm/sec. air velocity
Four pulses

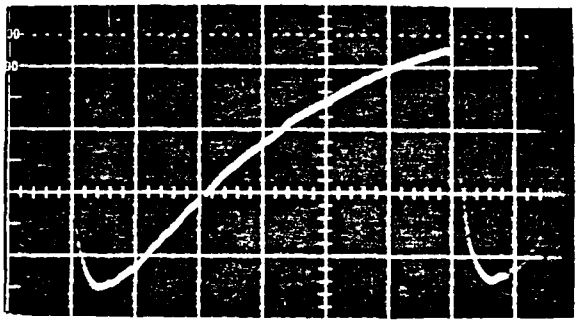

Horizontal .5 sec/div.
Vertical 65°C/div.
160 cm/sec. air velocity
Four pulses

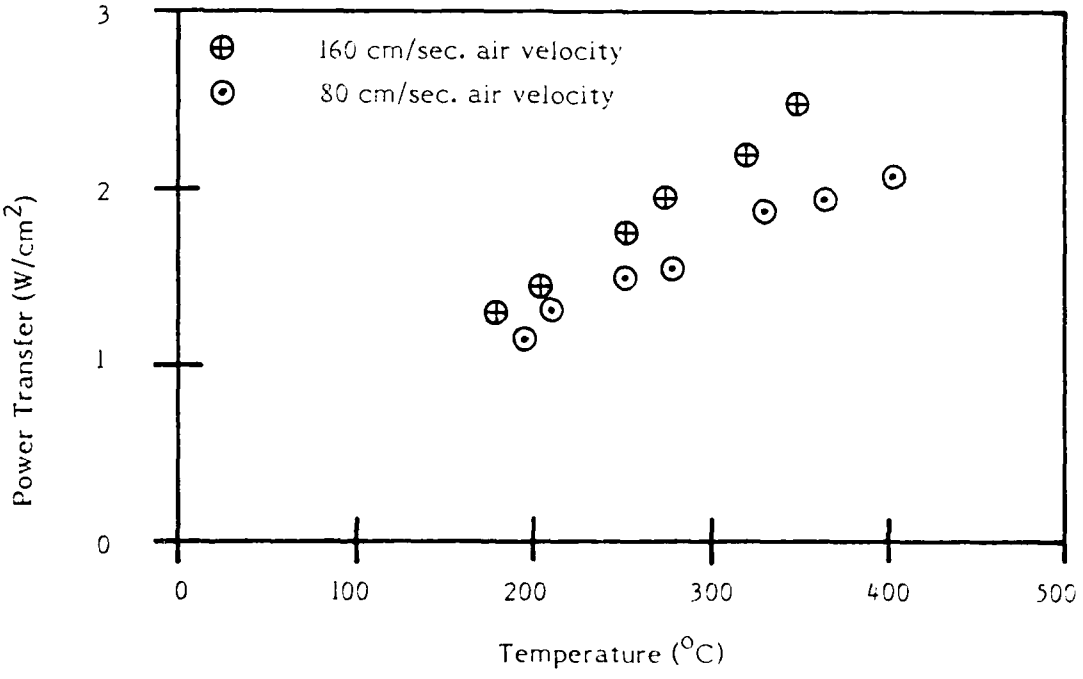

Fig. 4.15 Gas Cooling (Air Only) of Laser Test Cell
One Mil Stainless Steel Foil

The first geometry considered used two flat spray nozzles spaced on a 4.4 cm center. Flow conditions were established and the power density in the e-beam was slowly increased until an unstable operating condition, as indicated by a sharp increase in the thermocouple reading, was encountered.

The burst length was kept to ten shots so that in the event of a temperature instability the foil would not be destroyed. The 0.10 second run time was more than sufficient for this thin foil to come to thermal equilibrium. The data summary is shown in Table 4.2. Then the system was set to known unstable conditions and operated until the foil was destroyed. A photograph of the foil is shown in Fig. 4.16. The area of most intense heating have been outlined in the accompanying sketch and show that the cooling is inadequate in the center of the system. On the absolute centerline the single supporting rib intercepted the electron beam and the foil remained cold.

It was evident that mixing of the two nozzle flows was not occuring and that a "dead" space existed between the two flow streams. Fig. 4.17 shows a second failed foil, however, in this case the aerosol flow was not turned on in order to demonstrate that the previous beam pattern was not as a result of non uniform deposition by the electron beam.

An alternative configuration was attempted with the nozzles convergent at a 7^{o} slight angle to the centerline. The stability results were similar to the previous results and are tabulated in Table 4.3. A photograph of a foil is shown in Fig. 4.18. The angle of injection was obviously too large with the center of the foil being cooled and the outside unaffected and thus not cooled by the flow. A single nozzle was also mounted directly on the centerline of the system. Cooling for this case was considerably more uniform than the previous two cases. A photograph of the foil used for this test is shown in Fig. 4.19 and a table illustrating performance is given in Table 4.4.

For the data described above, the foil thickness and the beam kinetic energy was such that more than 90% of the energy was deposited in the first foil with on a small portion being deposited in the second foil.

TABLE 4.2

Test Data: Nozzle Configuration - 2 Full Cone Nozzles

Power Density	Water Rate	Flow Velocity	Stability
90 W/cm^2	5.2 gm/sec.	418 cm/sec.	stable
110W/cm^2	5.2 gm/sec.	418 cm/sec.	unstable
110 W/cm^2	10.5 gm/sec.	466 cm/sec.	stable
132 W/cm^2	10.5 gm/sec.	466 cm/sec.	unstable
132 W/cm^2	10.5 gm/sec.	790 cm/sec.	stable
160 W/cm^2	10.5 gm/sec.	790 cm/sec.	marginally unstable

Heating of first foil

Foil: 3 mil Titanium

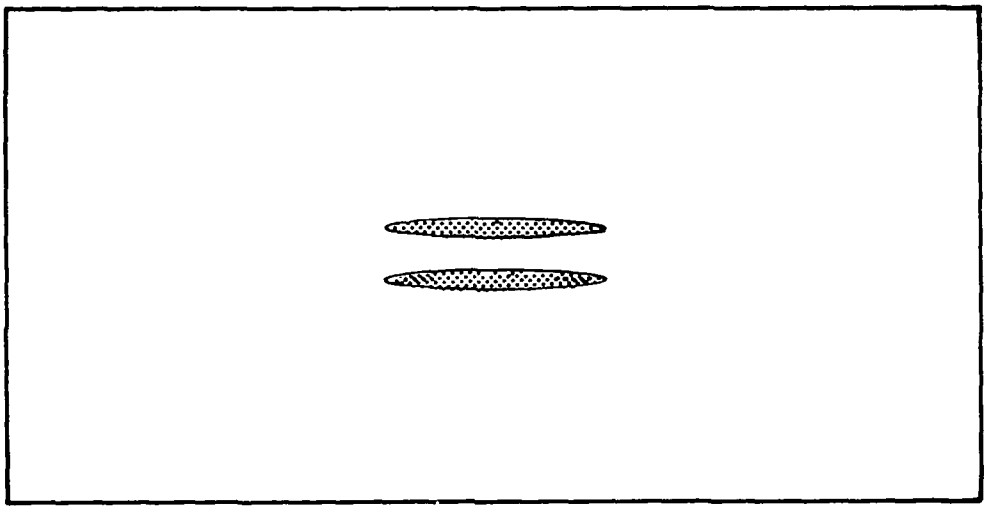

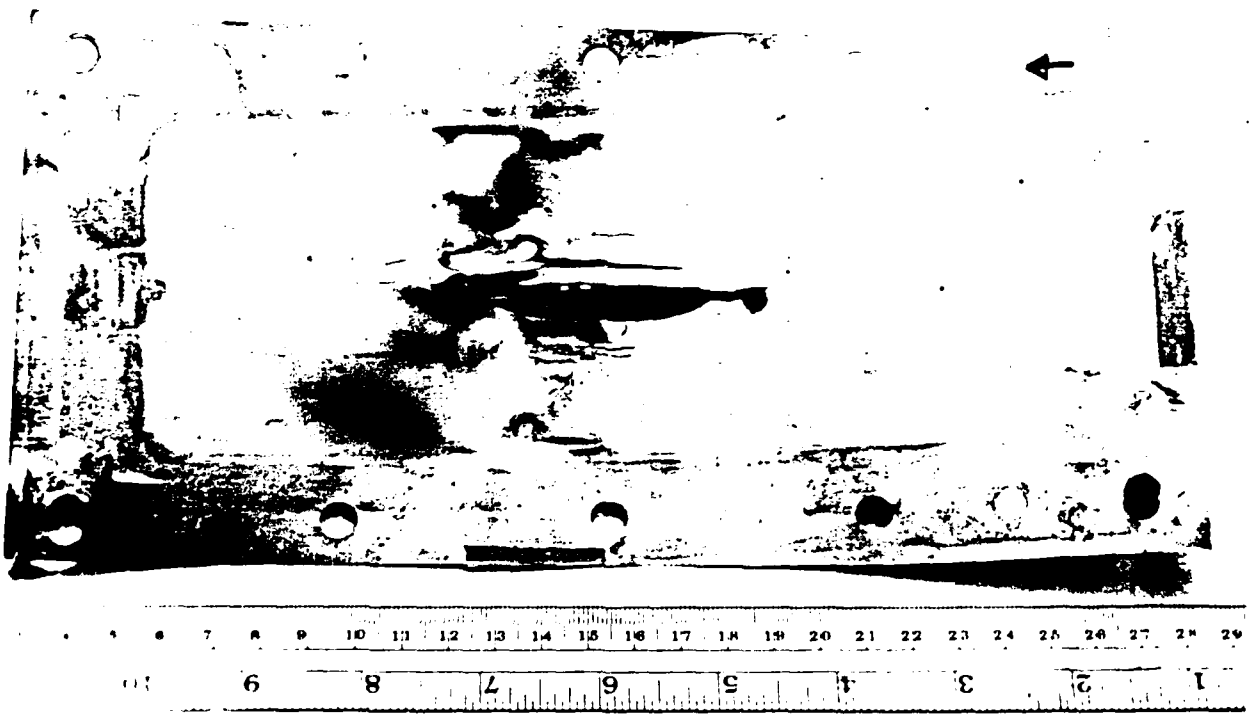

Fig. Two Flat Spray Nozzles

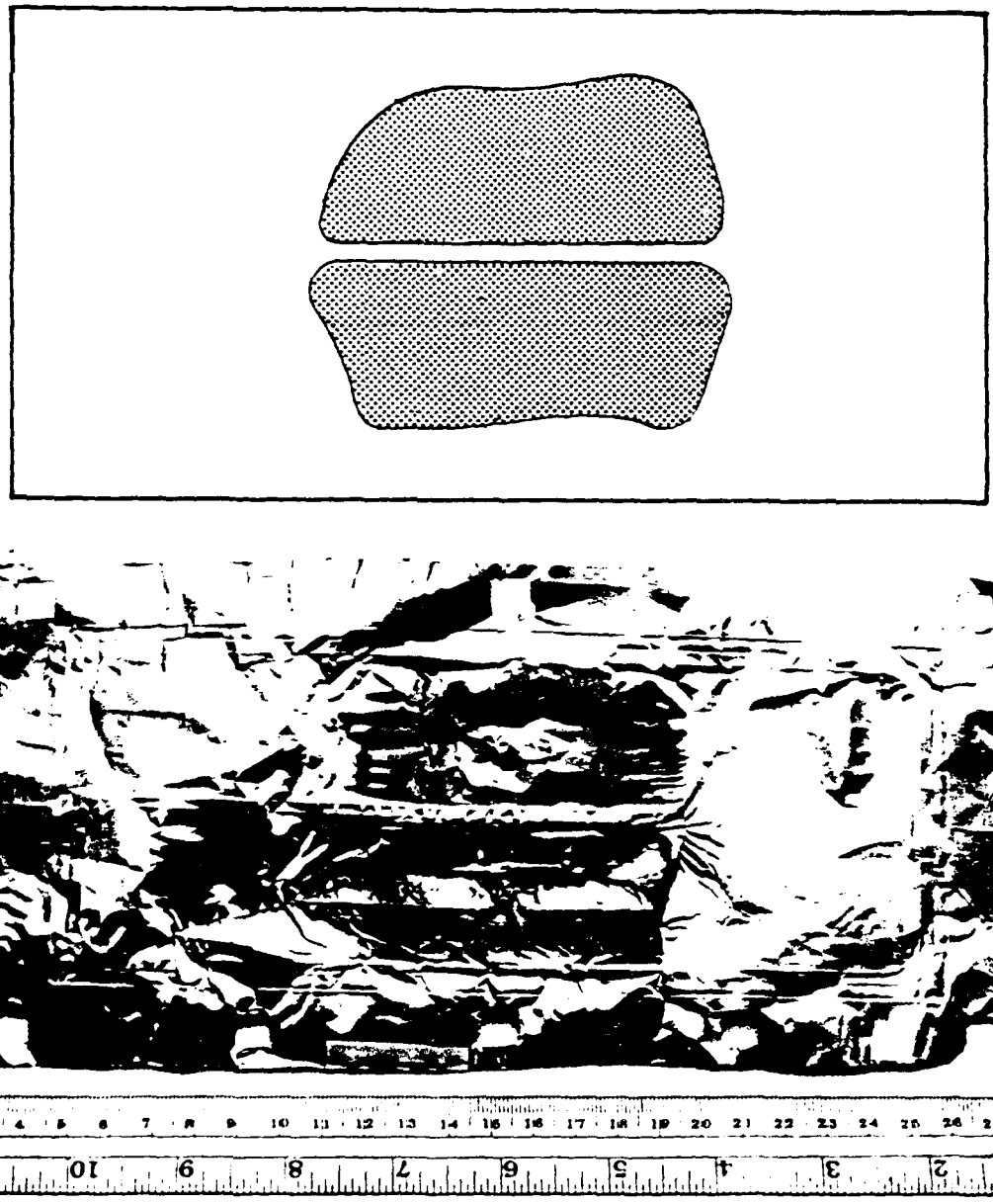

Fig. 4.17 Failed Foil; No Aerosol Cooling

TABLE 4.3

Test Data: Nozzle Configuration - 2 Flat Spray-Angled 7° Toward The Centerline

Power Density	Water Rate	Flow Velocity	Stability
90 W/cm^2	11 gm/sec.	624 cm/sec.	stable
90 W/cm^2	10.5 gm/sec.	710 cm/sec.	stable
110 W/cm^2	10.5 gm/sec.	710 cm/sec.	marginally stable
110 W/cm^2	12.6 gm/sec.	714 cm/sec.	stable
130 W/cm^2	12.6 gm/sec.	714 cm/sec.	unstable

Heating of first foil

Foil: 3 mil Titanium

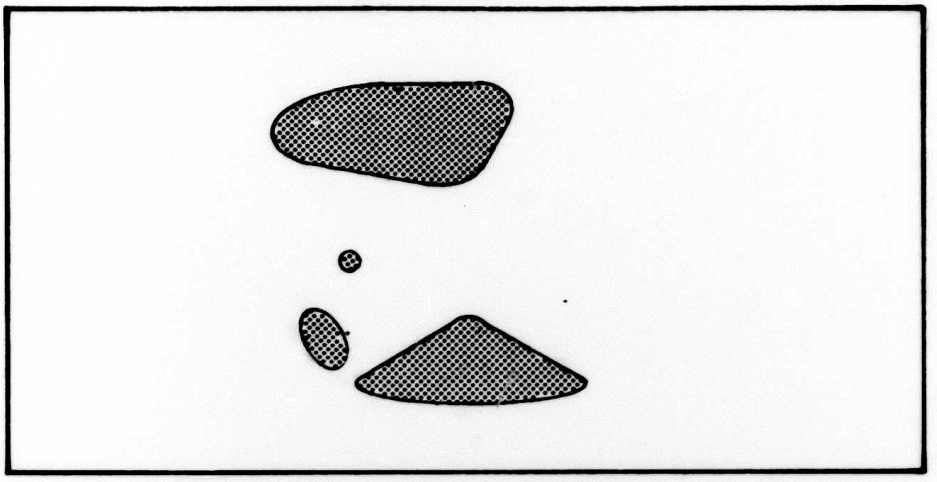

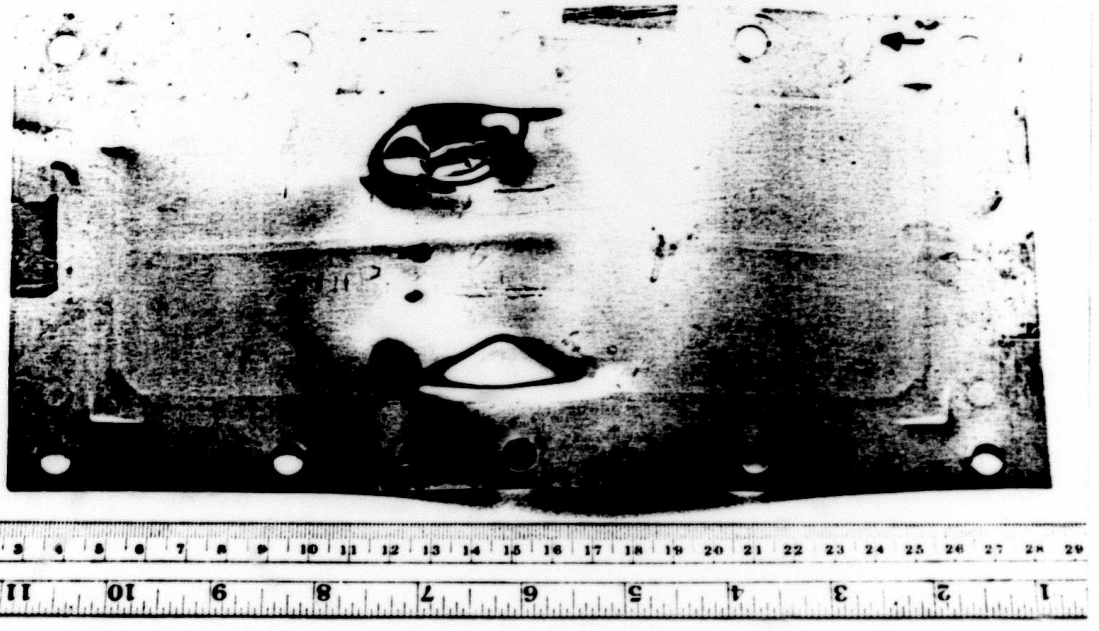

Fig. 4.18 Failed Foil; Two Round Spray Nozzles Convergent at a 7° Angle to the Center Line

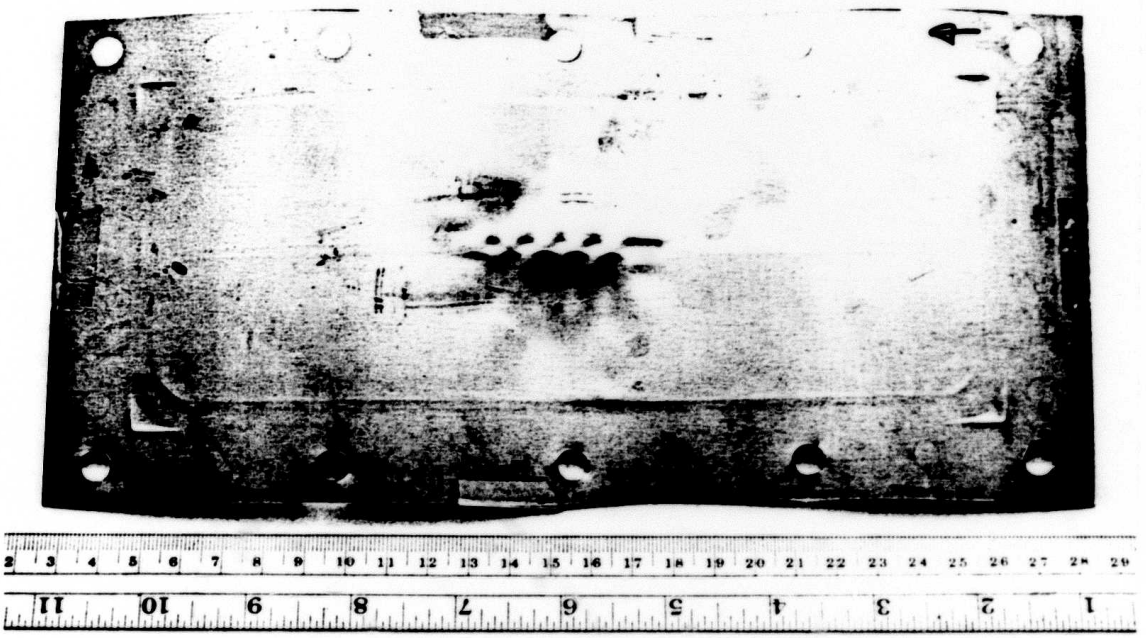

Fig. 4.19 Aerosol Cooling with Single Round Spray Nozzle Mounted on the Center Line

TABLE 4.4

Test Data: Nozzle Configuration 1 Full Cone Spray On Center

Power Density	Water Rate	Flow Velocity	Stability
132 W/cm^2	8.4 gm/sec.	385 cm/sec.	stable
160 W/cm^2	8.4 gm/sec.	385 cm/sec.	*marginally* unstable

Heating of first foil

Foil 3 mil Titanium